



**Deutsches Zentrum  
für Luft- und Raumfahrt**  
German Aerospace Center

**DB Cargo, Crosswind Investigation on the Great Belt Bridge**  
*Seitenwinduntersuchung auf der Großer-Belt-Querung:*

**Report**

<b>Project</b>	<b>Crosswind Investigation on the Great Belt Bridge</b>
<b>Starting date</b>	15/12/2021
<b>End Date</b>	15/09/2022
<b>Client</b>	DB Cargo AG
<b>Authors</b>	Dr. James Bell, Dr. Arne Henning
<b>First Version Date</b>	29/07/2022
<b>Current Version Date</b>	27/09/2022
<b>Version</b>	2.0

## Contents

Contents .....	3
Introduction .....	4
Objective .....	4
DLR FR8-LAB .....	4
Experimental Setup .....	4
Measurement Campaign .....	4
Test Wagon Configuration .....	4
Test Route .....	6
FR8-LAB Codification .....	7
Measurement Systems .....	7
Surface Pressure .....	7
Data Acquisition System .....	9
Power Supply .....	10
Real-time Analysis .....	11
Weather Station Data .....	13
Wind-Tunnel Calibration .....	15
Concept .....	15
Wind-Tunnel Experimental Setup .....	15
FR8-LAB wind-tunnel configuration .....	15
Test Conditions .....	18
Pressure Measurement .....	18
Flow Visualization .....	19
Calibration Methodology .....	22
Pressure Characteristics .....	22
Determination of Magnitude .....	23
Calibration Robustness .....	25
Application of Calibration .....	25
Results .....	26
System Functionality .....	26
Calibration Example .....	28
Validation .....	30
Time-Varying Crosswind .....	33
Individual Insight .....	33
General Crosswind Characteristics .....	36
Conclusions .....	40
Appendix .....	41

## Introduction

### Objective

The German Aerospace Center (DLR) has been commissioned by DB Cargo to carry out a detailed measurement campaign. The aim of the work is to measure the time-varying atmospheric wind - including gusts - that freight trains are exposed to in typical operation travelling over the West Bridge of the Great Belt Fixed Link between the Funen und Zealand islands in Denmark.

These measurements were performed using the DLR FR8-LAB measurement container, a 'swap-body' fitted with a self-contained data acquisition, power supply and a communication system that can be transported on normal operating freight-trains. The FR8-LAB was developed in 2021 as an experimental platform for research into the safety, efficiency and performance of freight transport, as part of the EU Shift2Rail, FR8RAIL IV research project. A measurement set-up from DB Systemtechnik (DB ST), that can record the time-varying air velocity with ultrasonic anemometers (USA) was also installed for some of the measurement campaign, taking measurements in parallel.

### DLR FR8-LAB

The full-scale experiments were performed using the DLR FR8-LAB measurement container shown in Figure 1. Time-varying surface-pressure measurements are used to derive the transient wind that the container is exposed to. A separate reduced-scale model wind-tunnel experiment was performed to determine calibration data to associate the measured surface-pressure to wind speeds the container is exposed to during transport on the freight train across the bridge.



Figure 1: The DLR FR8-LAB loaded on a wagon

## Experimental Setup

### Measurement Campaign

Measurements were taken across the bridge from January 10<sup>th</sup>, 2022 to March 4<sup>th</sup>, 2022. During this campaign, a range of weather conditions were captured, however in the scope of this project, crosswind was the primary focus. Over 70 bridge crossings were successfully measured, resulting in over 150GB of measurement data.

### Test Wagon Configuration

The DLR FR8-LAB was loaded onto a test-wagon consist, presented in Figure 2. The FR8-LAB was positioned on a 6-axle articulated - Sggmrs 714 wagon (Figure 3) – coupled with an additional 4-axle Sgns 691 wagon (Figure 4). This configuration resulted in a minimum gap in front and behind of the measurement container of ~17m & ~29m respectively. This ensured the FR8-LAB was ideally positioned in order to take robust cross-wind measurements – being as exposed as possible to crosswind, rather than being affected by the locomotive/other containers in front of it, within the train consist.



Figure 2: The FR8-LAB loaded on the test-wagon consist for the Great Belt Bridge experimental campaign

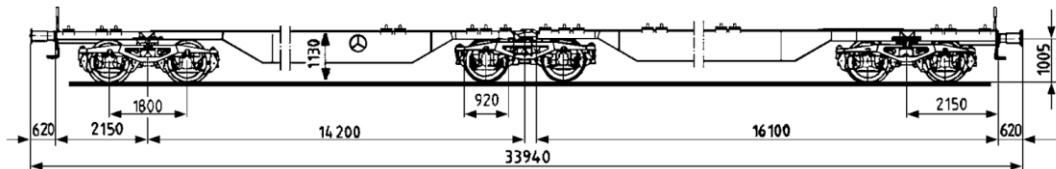


Figure 3: Sggmrs 714 six-axle articulated wagon, source:

[https://nl.dbcargo.com/resource/blob/1430008/9767e97bb070ccb77efd84e7d64948/freight\\_wagon\\_catalog\\_v2011-data.pdf](https://nl.dbcargo.com/resource/blob/1430008/9767e97bb070ccb77efd84e7d64948/freight_wagon_catalog_v2011-data.pdf)

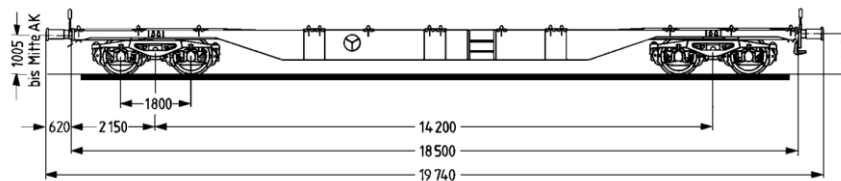


Figure 4: Sggmrs 691 4-axle wagon source:

[https://nl.dbcargo.com/resource/blob/1430008/9767e97bb070ccb77efd84e7d64948/freight\\_wagon\\_catalog\\_v2011-data.pdf](https://nl.dbcargo.com/resource/blob/1430008/9767e97bb070ccb77efd84e7d64948/freight_wagon_catalog_v2011-data.pdf)

From February 7th, 2022 the DB ST experimental setup was also installed & measurements made in parallel. For this setup, both the DLR FR8-LAB, and the DB ST ultrasonic anemometers (USAs) measurement systems were running in parallel. During parallel measurement, the wagon configuration was changed: The FR8-LAB was positioned on the same 6-axle articulated - Sggmrs 714 wagon coupled with 3 additional 4-axle Sgns 691 wagons together (Figure 5).

This configuration resulted in a minimum gap in front and behind of the FR8-LAB of ~10m & ~66m. In this case, the ~10 m gap results in the FR8-LAB being less isolated, and more likely to be affected by the locomotive/other containers if they are only 10m in front of the FR8-LAB. In contrast, the ~66m gap is very large, and again provides an isolated FR8-LAB, very suitable for being exposed to crosswind, and taking robust measurements. The gap (10 or 66m) in front of the container depends on direction which the train consist travels. Logs supplied by DB Cargo on the train consist for a given measurement show the test-wagon consist travelled in both directions, meaning both gap configurations were measured.

The DB ST ultrasonic anemometers (USAs) were located centrally in the middle Sgns 691 with 9m spacing between them. Resulting in distances of ~45m and 36m from the USAs respectively to the closest end of the FR8-LAB (Figure 5). Details of the DB ST setup and results can be found in the "220211 Belt-Bridge\_info\_prelim" presentation from DB ST.



Figure 5: Test-wagon configuration during parallel measurements of DLR FR8-LAB and DT ST USAs, Source: DB ST "220211 Belt-Bridge\_info\_prelim" presentation

## Test Route

The full test-route that the freight-trains carrying the FR8-LAB test wagons travelled each trip, as illustrated in Figure 6, was between: Taulov / Fredericia (Fa) - Høje Taastrup (Htå)

The area of focus for measurements was the Great Belt Bridge, illustrated in Figure 7 between: Nyborg (Ng) – Korsør (Kø), specifically the section where the track is on a bridge section above the water between Nyborg and the small island of Sprogø, to the east of which, the track goes into a tunnel.

The freight trains carrying the FR8-LAB test wagons performed this route ~4 times (2 round trips) per day, crossing the bridge at approximately 3am, 6am, 12pm and 9pm. Measurements made throughout the day enabled different environmental conditions to be captured over the 8 weeks of the campaign.



Figure 6 The full test route of Fredericia (Fa) - Høje Taastrup (Htå),

Source: <https://www.openrailwaymap.org/?style=standard&lat=55.66906586432122&lon=10.960235595703125&zoom=9>



Figure 7 The area of focus for measurements was the Great Belt Bridge between Nyborg (Ng) & Korsør (Kø) Source:

<https://www.openrailwaymap.org/?style=standard&lat=55.31908502686636&lon=10.970020294189453&zoom=12>

## FR8-LAB Codification

The DLR FR8-LAB measurement container is a 'swap-body' that has been certified/codified (illustrated in Figure 8), and can be transported on normal operating freight-trains:

- ILU-Code: DLRA 864512 2
- WB-Type: WK 7.7 STG
- Length: 7820mm
- Height: 2750mm
- Width: 2550mm
- Gross Weight: 3.9t
- Codification: C48 S48, 006 . 001612 . 5W1229520



Figure 8: FR8-LAB certification details

## Measurement Systems

### Surface Pressure

The primary measurements are time-resolved (up to 1000Hz) surface-pressure measurements at up to 330 positions on the container (Figure 9, Figure 10). This corresponds to >200,000 samples per sensor, per bridge-crossing measurement. Pressure on the front and rear surface can be integrated and provide insight into the pressure drag. Longitudinal rows and rings along the side and roof of the container provide insight into the side force, yaw and roll moments. Surface-pressure measurements provide a direct measure of the effect that the airflow has on the swap body container at specific local measurement locations. Integration of the pressure over the surfaces provides an estimation of the global aerodynamic forces and moments acting on the container. The pressure measurements locations were selected to resolve the pressure gradients across the surface, and identify the pressure signature of complex turbulent flow structures like the recirculation regions in between containers and flow separation at the roof/sides. This enables accurate predictions of the forces and moments on the container and provides insight into the underlying causal flow physics.

The pressure is measured using individual  $\pm 4$  kPa Honeywell piezoresistive-silicon differential-pressure sensors at each measurement position. The sensors are temperature compensated, digital, with I2C communications, operating at 3.3V with 12-bit resolution and maximum acquisition rate of 2kHz. The reference side of each sensor is open to the interior pressure of the container. The container has in-direct (shielded) vents to the outside, which allows the inside of the container to maintain consistency with local atmospheric pressure.

Each pressure sensor is connected to a machined Acetal pressure manifold that has a path from inside the container to the external surface. On the external surface, a 40mm diameter, 1mm thick disc has a 0.6mm diameter hole through it, which expands after 5mm to a 1mm diameter hole of 25mm length, to which 1mm inner-diameter, 70mm silicone tubing connects to the sensor. This short tubing distance from measurement point to sensor enables a high frequency response. Additionally, the pressure sensors are fixed to custom printed circuit boards (PCB) that are fixed to metal brackets (mounted on the inside of the container to the pressure manifolds) using rubber vibration isolating elements; to reduce the effect physical vibrations have on the transient pressure measurements.

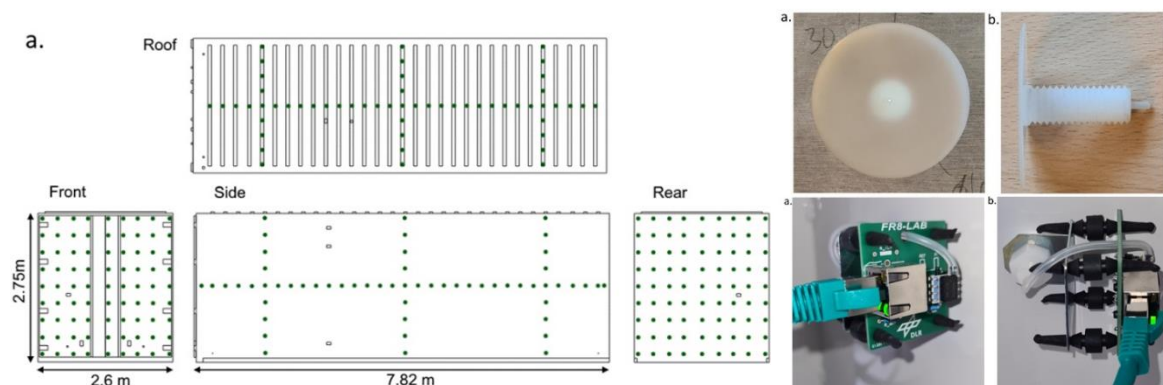


Figure 9: Surface pressure distribution, pressure manifolds, and printed circuit board with pressure sensor



Figure 10: External view of FR8-LAB, showing the outer part of the pressure manifolds

## Environmental Monitoring

Additional sensors measure the container's operating conditions and associate them to the measured surface-pressure and corresponding aerodynamic characteristics. A global navigation satellite system (GNSS) determines the location and the velocity over ground (VOG). Up to seven single-point LiDAR distance sensors with 40m range are located on the container's sides, roof and front/rear surface to quantitatively characterize the physical environment at high temporal resolution sampling rates of up to 1000Hz. Two wide-angle 75° field-of-view (FOV) thermal cameras (able to operate at night and in poor weather conditions) with 640 x 512 pixel resolution provide additional qualitative information on the local topography (Figure 11, Figure 12). Accelerometers, barometric pressure and temperature sensors measure the conditions inside the container.

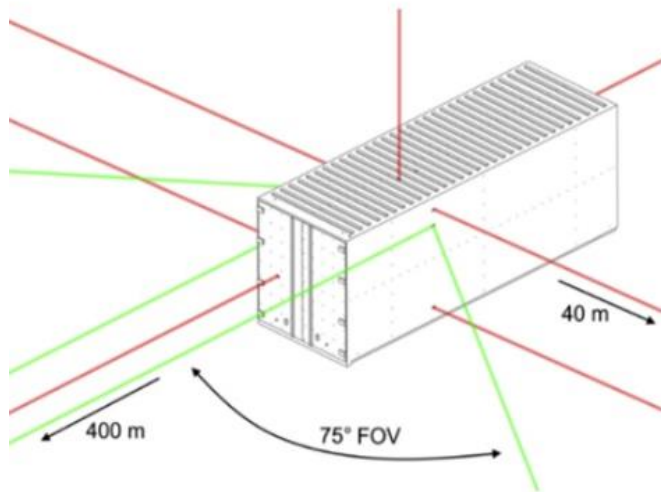


Figure 11: Environmental monitoring: 7 x LiDAR and 2 x Thermal cameras

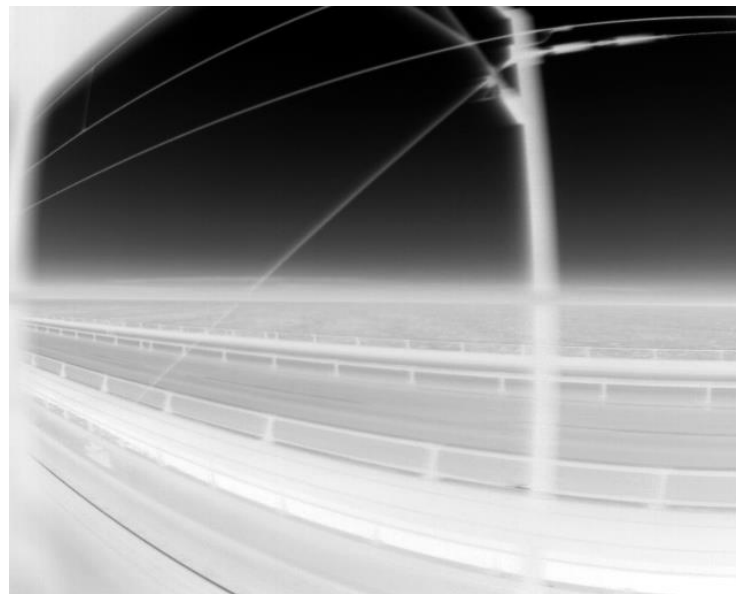


Figure 12: Example thermal camera image during a bridge-crossing measurement

### Data Acquisition System

A bespoke data acquisition system (DAQ) – consisting of both software and electronic component architecture – was developed for the FR8-LAB. Such a specific system was required due to the novel experimental requirements: high number of synchronized sensors, relatively high sampling rate, operating in a challenging environment (vibrations, heat/cold, moisture) with low overall power consumption. The DAQ system utilized an Internet of things 'IoT' hardware/software system architecture.

Clusters of up to 16 sensors (pressure, acceleration, temperature, distance) connected to multiple *Nucleo F767Zi* micro-controller nodes, that trigger and log data (Figure 13). Synchronized data is acquired simultaneously for the 16 sensors utilizing the I2C digital communications protocol run in parallel; 'bit-banging'. Each node then communicates the measurements to a central server Central Processing Unit (CPU) *Raspberry Pi*, using the User Datagram Protocol (UDP) communication

protocol that then collates and stores the measurements from all nodes using the real-time series database management software; *InfluxDB*. The clocks of the multiple nodes are synchronized using the precision time protocol (PTP), resulting in sensors from different nodes having temporal precision of ~1 microsecond. The data acquisition and synchronization was facilitated within a RIOT operating system running on the nodes. RIOT is an open source operating system intended for 'IoT' devices and microcontrollers. Programming in C/C++, multithreading and real-time functionality is supported in RIOT, making it well-suited to being used in the data acquisition system of this novel experiment. Real-time analysis of the measurement system for system health monitoring and data sanity checking is performed using *Grafana*, an open-source data analytics program accessed remotely over the 4G/LTE connection.

The global position, and velocity over ground (VOG) that the container is moving at - as part of the entire freight-train consist - is measured by two Global Navigation Satellite Systems (GNSS). The GNSS is connected to the same industrial, weatherproof SENCITY OMNI-S antenna mounted on the roof. The antenna is dual-purpose, also facilitating a 4G/LTE mobile connection.

Remote-access to the system is possible through the 4G/LTE connection. This enabled data management, sanity checking, trouble-shooting, and direct manual control of systems if necessary. In addition, the embedded system contained multiple 'intelligent' software sub-systems, such as automatic system idle and data-acquisition triggers based on speed, geofencing. For the standard bridge-crossing measurement, the data acquisition was triggered using a geofence based on longitude – between 10.58 (Langeskov) and 11.35 (Slagelse). This ensured there was enough time either side of the bridge for the system to start up, and take some additional data for sanity checking, before the critical data during the bridge-crossing.

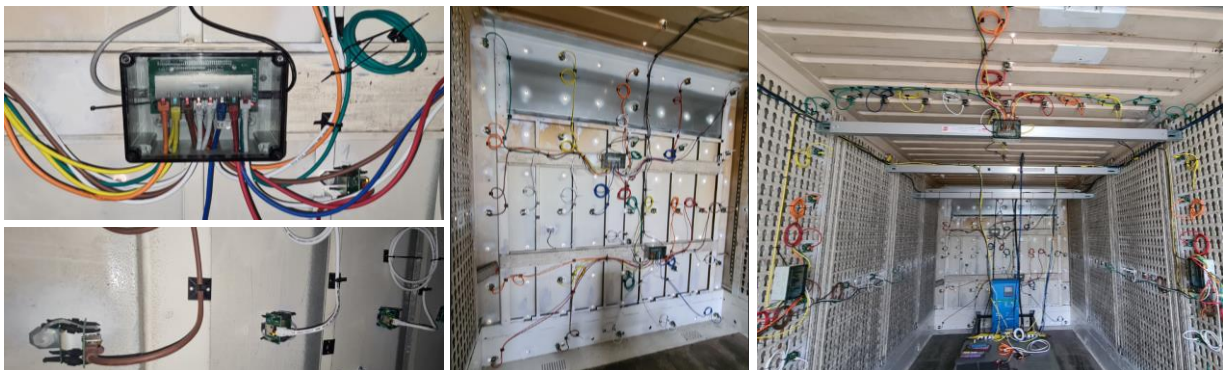


Figure 13: Measurement equipment inside the FR8-LAB

## Power Supply

The core of the power supply system is 16 individual *Sun Power VRM 6V 200Ah* absorbent glass matt (AGM) batteries. AGM batteries were specifically used to be able to best withstand vibration, shocks and tipping over. Combined, the batteries provide up to 20kWh, which at a conservative total system requirement of 100W, corresponds to approximately 8 days of possible system duration. The roof of the FR8-LAB is covered in 30 individual 50W solar panels (Figure 14) that recharge the batteries and extend the system duration. An external power socket on the door enables manual charging by cable if necessary - this was performed at Taulov during the experimental campaign, as minimal sun and solar charging was possible during winter in Denmark.



Figure 14: Solar panels fitted on the roof of the FR8-LAB

## Real-time Analysis

Real-time analysis capability was achieved, utilizing the 4G/LTE remote-access connection. This enabled data sanity and system checking, manual control, troubleshooting with *Grafana* and *InfluxDB*. Primary measurement data, such as specific surface pressure sensors, LiDAR, acceleration, location and speed could be observed and assessed in real-time (Figure 15). In addition, open-source weather *OpenWeather API* (<https://openweathermap.org/api>) associated to the current latitude and longitude was also assessed in real time (Figure 16), to assist in interpreting the measurements (e.g. confirming crosswind was present). The power supply was also monitored online, using the Victron Energy: Power management system online capability with 4G/LTE connection (Figure 17).

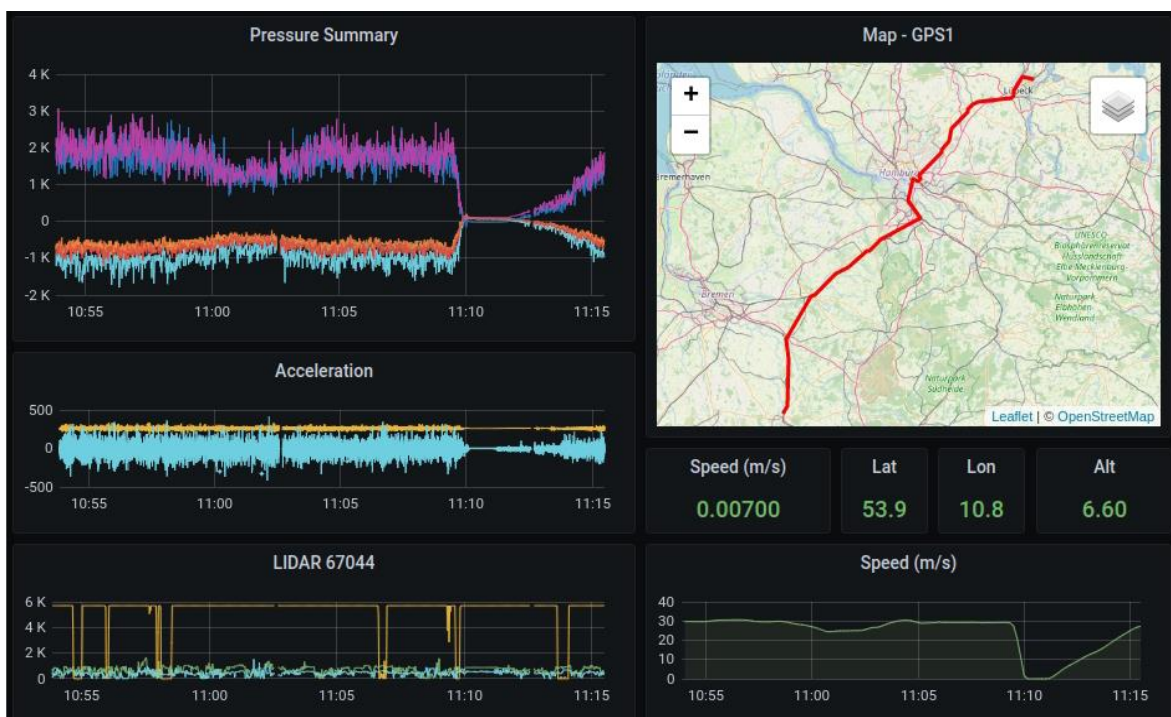


Figure 15: Real-time measurement analysis GUI using Grafana

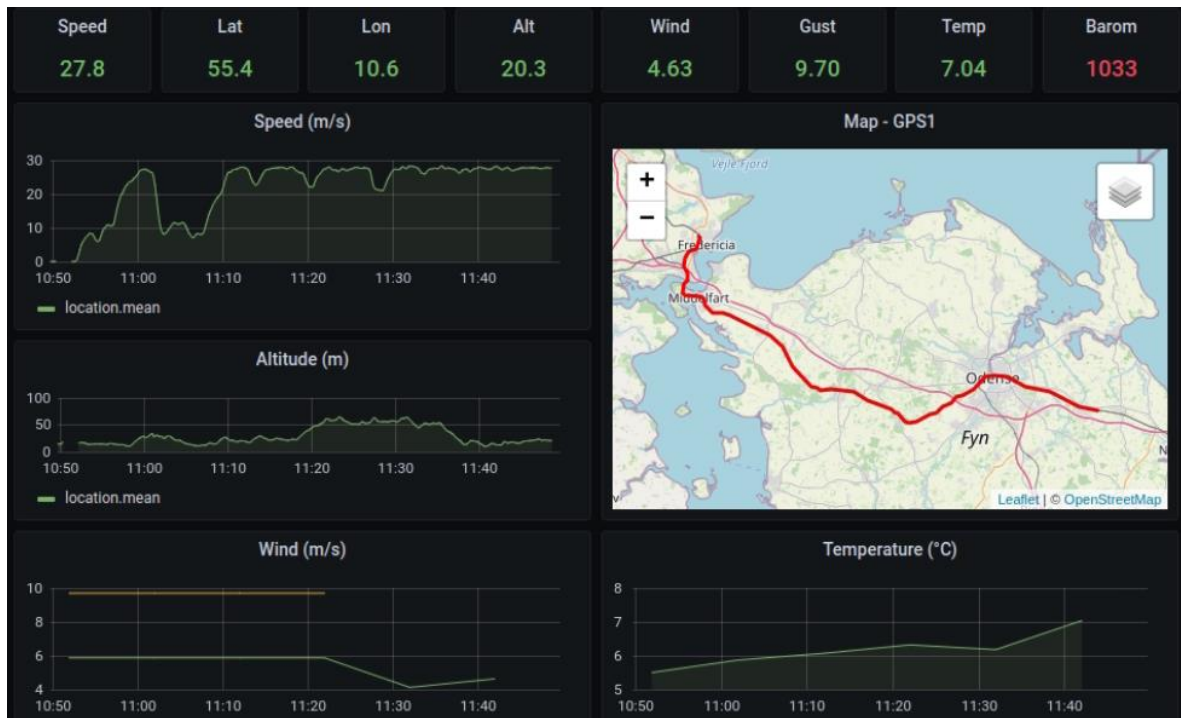


Figure 16: Real-time weather using Grafana and data from the OpenWeather API

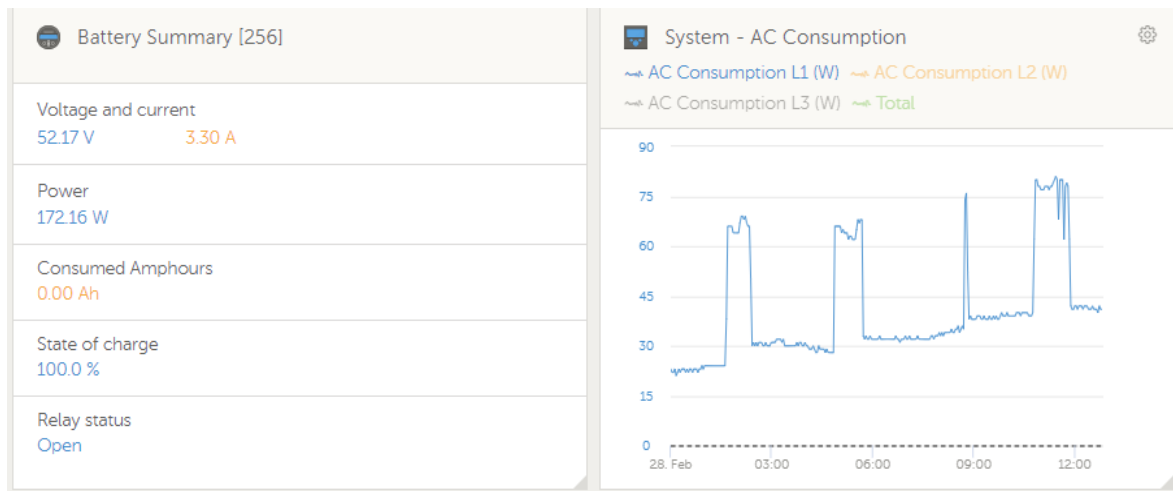


Figure 17: Real-time power management monitoring using Victron Energy

## Weather Station Data

In addition to the ultrasonic anemometer measurements performed in parallel by DB ST, local weather-station data was sourced to validate the wind velocities derived from the FR8-LAB measurements. As no data was readily available directly on the Great Belt Bridge, the most appropriate alternatives were sourced. The best, in terms of proximity, and similarity of environment (e.g. exposed on the water) was the Omø weather station data “Omø Fyr, ID 06151”, available through the Danmarks Meteorologiske Institut (DMI). To assess the suitability of this station, additional simulated and interpolated (from multiple nearby weather station) sources were also assessed. The simulated data purchased from meteoblue AG; with two different weather models obtained: NEMS4 from NOAA, and ICONEU from DWD:

([https://www.nws.noaa.gov/ost/CTB/mts-arch/CFSv3-Plan-Mt-082511\\_files/Lapenta.pdf](https://www.nws.noaa.gov/ost/CTB/mts-arch/CFSv3-Plan-Mt-082511_files/Lapenta.pdf),  
<https://www.dwd.de/DE/leistungen/modellvorhersagedaten/modellvorhersagedaten.html>,

respectively). The interpolated data consists of measured data from multiple local weather stations interpolated over a 10 km grid – provided by DMI - with the closest interpolated position to the bridge being used. The multiple sources are illustrated relative to the Great Belt Bridge in Figure 18.

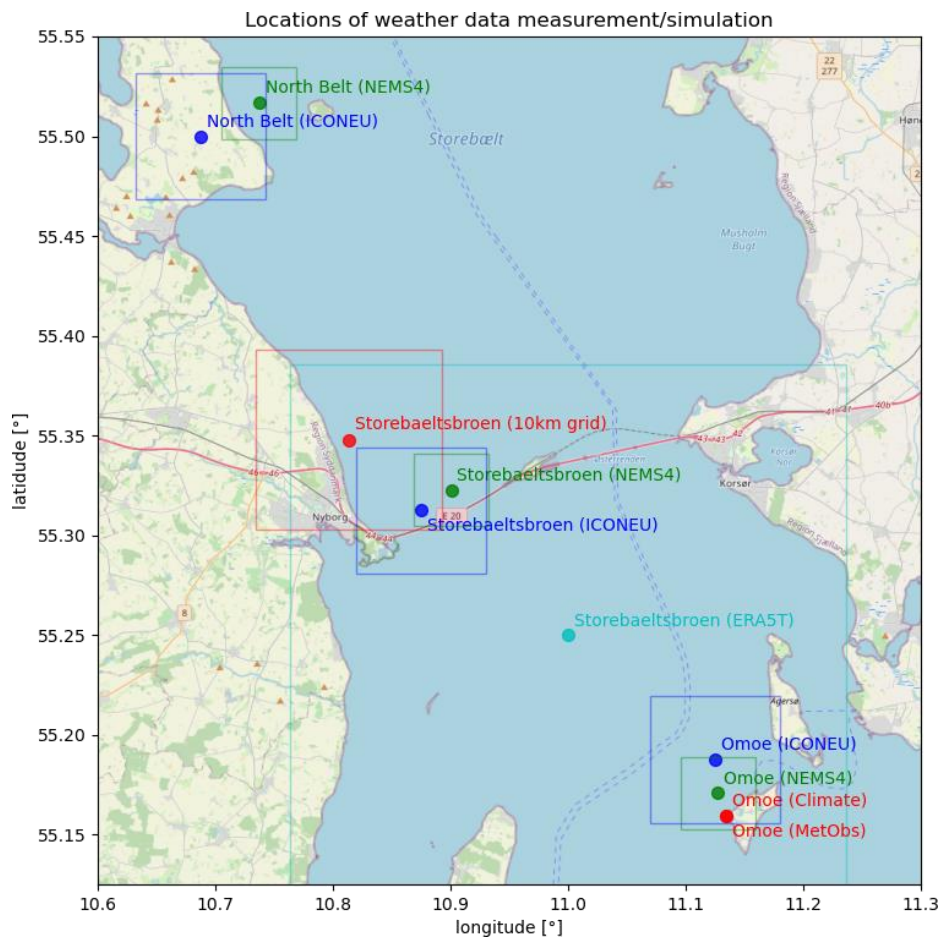


Figure 18: Map illustrating different weather data sources

The average and maximum wind speed measurements of the Omø weather station data compare well with the simulated and the interpolated data at the approximate position of the Great Belt Bridge (Figure 19, Figure 20). Thus, the Omø weather station data is representative of the estimated wind at the bridge. Further the data available from the DMI at Omø has a resolution of 10 minutes, which is higher than most other available sources. Thus, the Omø weather station data from DMI was determined as most suitable as the alternative validation data source.

The height of velocity measurement of the Omø weather station is 10m (<https://confluence.govcloud.dk/pages/viewpage.action?pagelid=26476616>). In contrast, the relative height of the Great Belt Bridge is > 18m (<https://storebaelt.dk/en/about-storebaelt/facts-history/>). Thus, although the Omø is the best in terms of similar environment (being exposed on the water), some differences in wind conditions can be expected, due to the different height above sea level.

The available data from the Omø weather station, with 10 minute temporal resolution is:

- **Mean wind speed:** 10 minutes' mean measured 10 m over terrain (<https://confluence.govcloud.dk/pages/viewpage.action?pagelid=26476616>)
- **Gust (3s) wind speed:** 10 minutes' highest 3 seconds mean wind speed measured 10 m over terrain (<https://confluence.govcloud.dk/pages/viewpage.action?pagelid=26476616>)

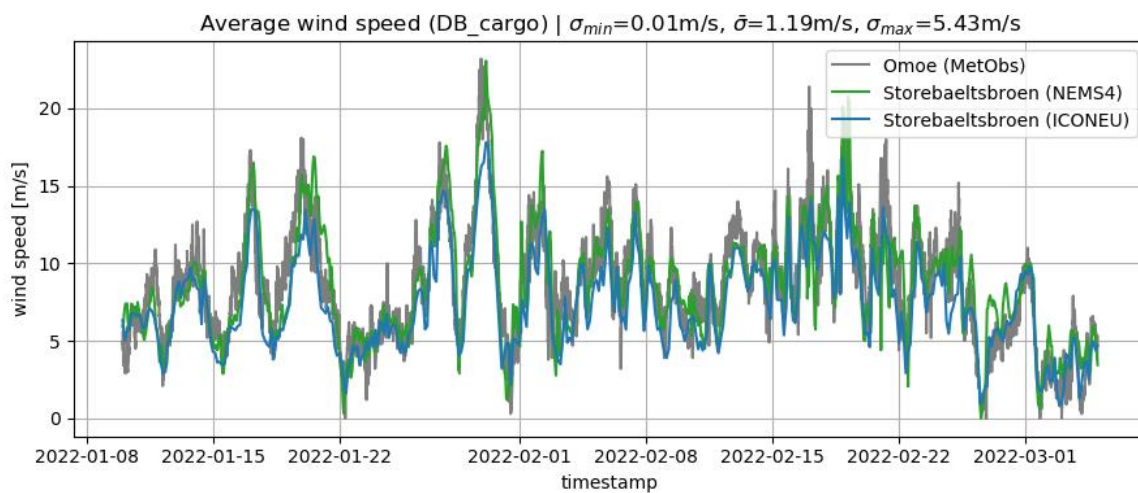


Figure 19: Average wind speed at Omø, simulated @ bridge: (NEMS4, ICONEU models)

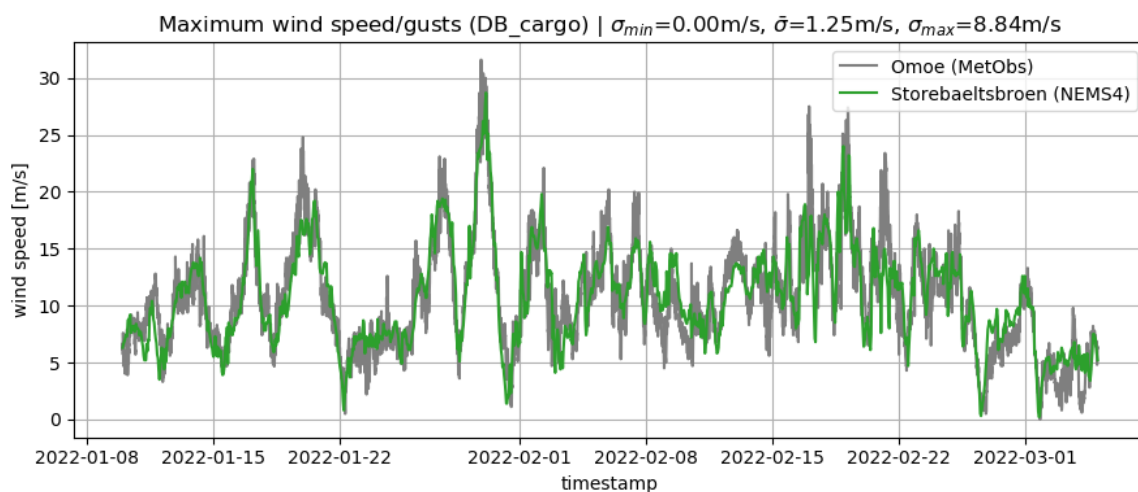


Figure 20: Max wind speed at Omø, simulated @ bridge: (NEMS4, ICONEU models)

## Wind-Tunnel Calibration

### Concept

Surface pressure measurements - analogous to those obtained in full-scale on operational freight trains on the FR8-LAB - were obtained in a 1:15 reduced-scale wind-tunnel experiment. The FR8-LAB model was statically oriented at different angles in the wind-tunnel, exposing it to oncoming flow with different discrete yaw angles – modelling exposure to crosswind.

The relationship between the available information in the wind-tunnel experiment, the full-scale experiment, and their connections are illustrated in Figure 21. The general concept is that surface pressure on the different surfaces of the container exhibit different characteristics (high pressure, low pressure), that vary in different ways (increase, decrease, remain constant) for different yaw angles that the FR8-LAB is exposed to. Characterizing this surface pressure response to known yaw angles in the wind-tunnel experiment, can be used to determine what the unknown yaw angle the FR8-LAB is exposed to in full-scale operation. To do this, the pressure at different surfaces is combined to create a calibration function, that can be applied to the full-scale data. This process is outlined and demonstrated in this section.

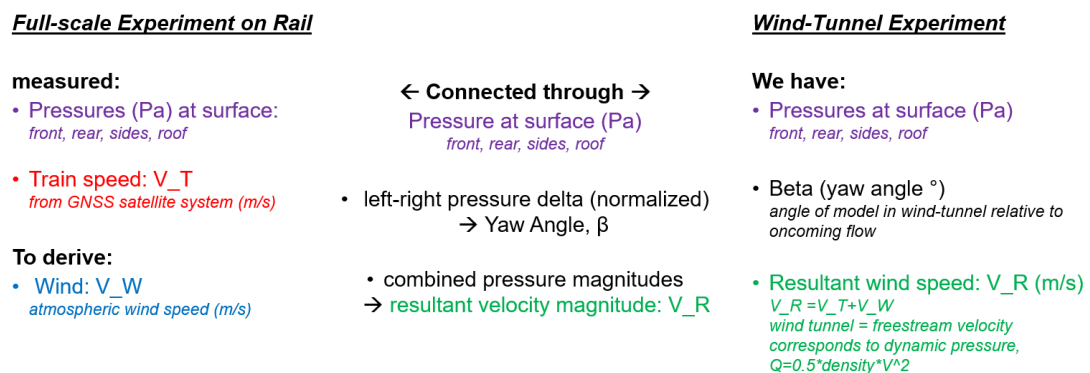


Figure 21: Calibration Concept Diagram

### Wind-Tunnel Experimental Setup

The wind-tunnel experiment was performed in the Crosswind Simulation Facility (SWG) at DLR Göttingen. An overview of the main functional components is provided in Figure 22 and Figure 23. The SWG is a closed-circuit wind tunnel (Göttingen-type) with a test-section of 2.4m x 1.6m x 9m (see Figure 24, Figure 25 & Figure 26). The 0.5MW compressor and the nozzle contraction ratio of 3.13 provides a maximum Mach number of 0.189 and a Reynolds-number of  $4.26 \times 10^6$  for a characteristic length of 1m. The flow speed within the test section can be varied from 2m/s up to 67m/s.

### FR8-LAB wind-tunnel configuration

For the FR8-LAB wind-tunnel experiment, the wind-tunnel was configured to have a splitter plate mounted to a computer-controlled turn-table in the wind-tunnel test-section floor. The 2380mm long, 1300mm wide rounded-corner splitter-plate was raised 195mm from the wind-tunnel floor, reducing the influence of the ground-boundary layer that exists on the floor of the wind-tunnel (that doesn't exist in full-scale operation of freight trains over the ground). The 1:15 scale test-model consists of a generic wagon with wheelsets with an adjustable length, in addition to dummy containers and a generic locomotive – used to vary the upstream gap configuration. The test-model is fixed above a 1:15 single-track ballast and rail, modelling a generic ground configuration that the freight train would typically operate above.

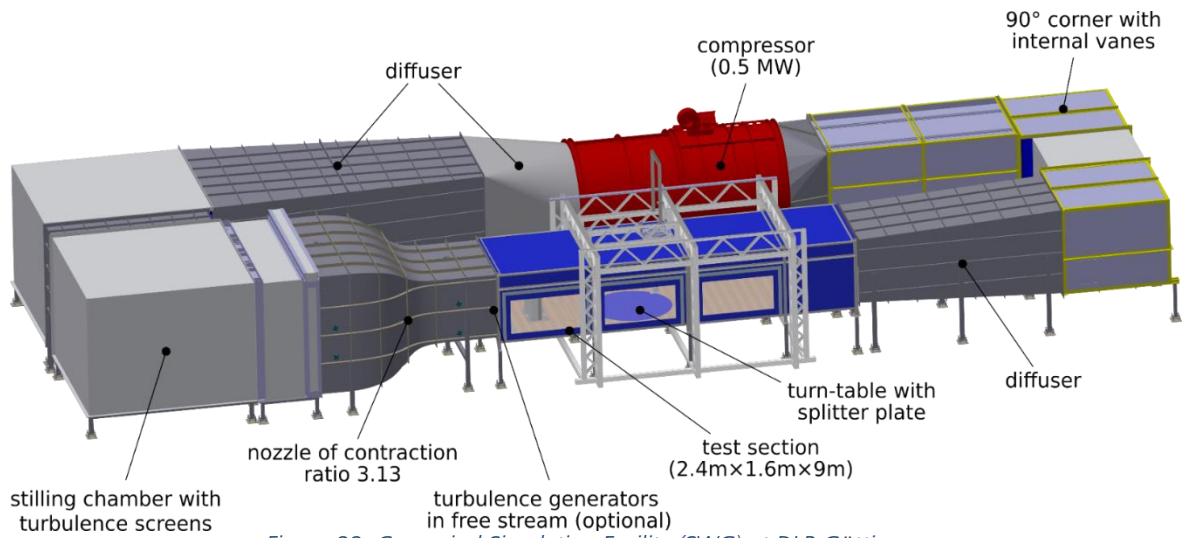


Figure 22: Crosswind Simulation Facility (SWG) at DLR Göttingen

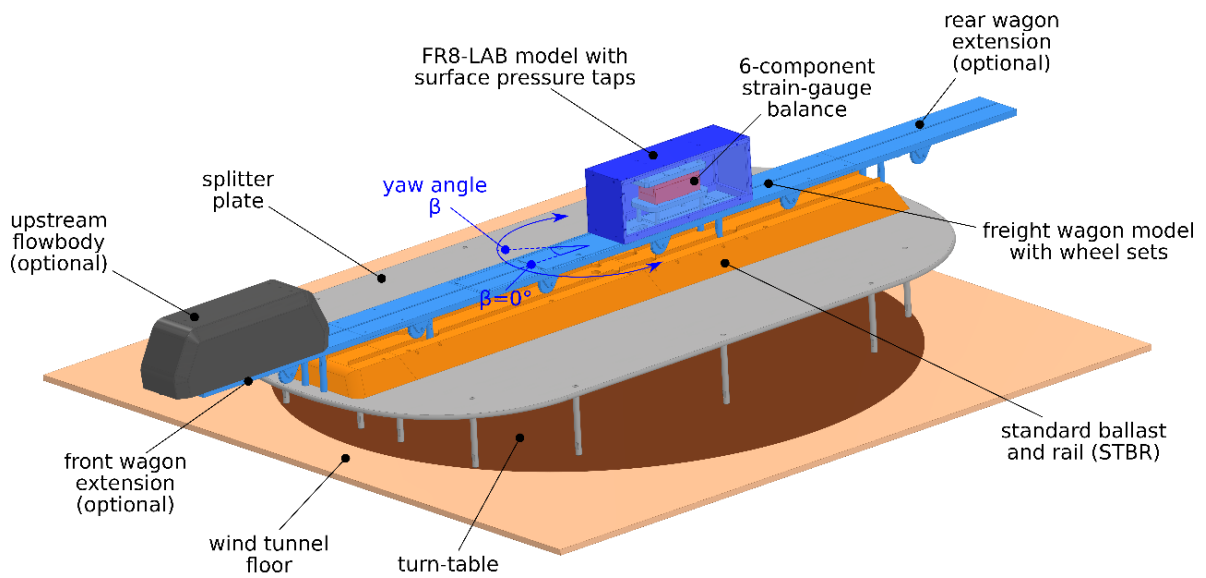


Figure 23: FR8-LAB wind-tunnel experimental setup



Figure 24: Photos of the FR8-LAB wind-tunnel experimental setup in different loading configurations

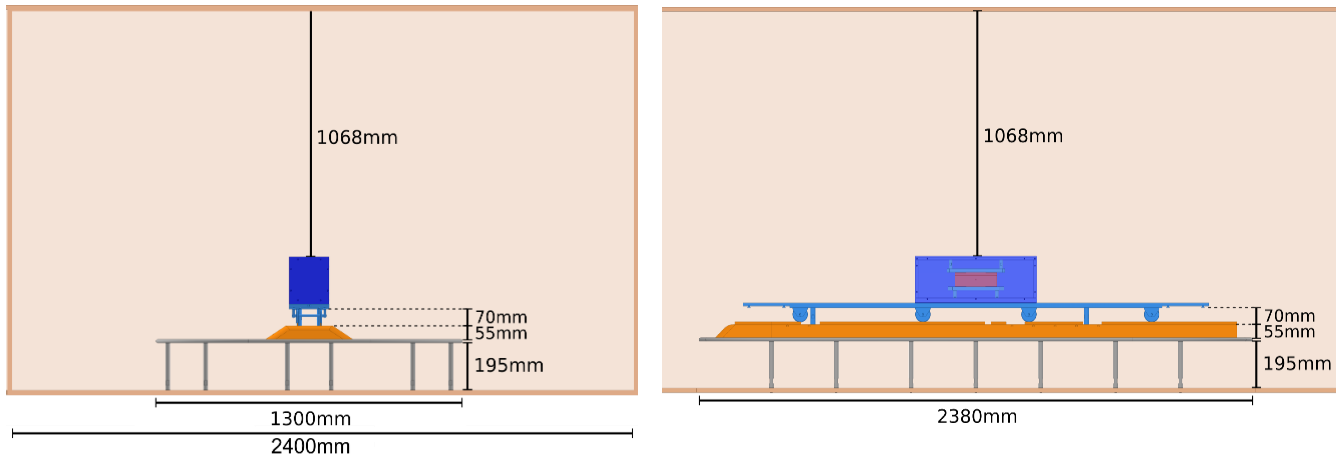


Figure 25: FR8-LAB wind-tunnel experimental setup diagram, front, side view

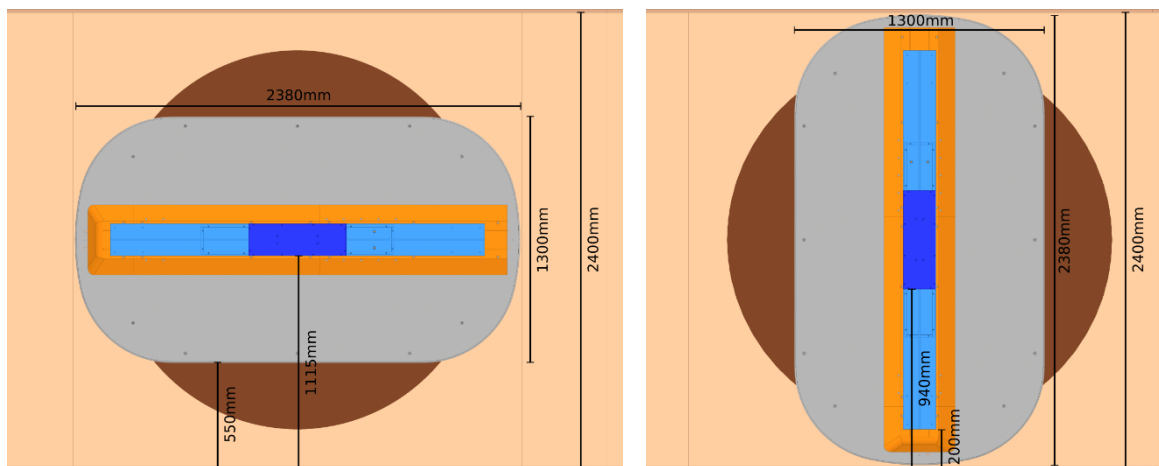


Figure 26: FR8-LAB wind-tunnel experimental setup diagram, top views 0, 90° yaw angle.

Additional turbulence generating elements were added in the wind-tunnel, 4m upstream of the model position in the test-section, to model different levels of freestream turbulence. Three different configurations (in addition to the default configuration of no elements) were modelled in the wind tunnel (illustrated in Figure 27):

- turb1: 11 bars, 0.04m width, 0.2 m spacing
- turb2: 5 bars, 0.04m width, 0.4 m spacing
- turb3: 5 bars, 0.08m width, 0.4 m spacing



Figure 27: Turbulence configurations added upstream of the model test-position, left-right configurations: turb1, turb2 and turb3

### Test Conditions

The wind-tunnel model of the container was statically yawed over a range of  $-90:90^\circ$ , mapping the relationship between changing surface pressure characteristics and different yaw angles (i.e. the known oncoming flow conditions). In addition to varying yaw angles, different conditions were tested:

- freestream velocity range of 10 to 60m/s, corresponding to Reynolds-numbers, of  $Re=1-6 \times 10^5$  respectively
- freestream turbulence intensities of ~1,3,4 and 5%
- different loading configurations: upstream locomotives/containers resulting in full-scale equivalent gaps of 0.23-17.8m.

Testing at these different conditions provides insight into the sensitivity of the calibration to conditions.

### Pressure Measurement

Surface-pressure measurements in the wind-tunnel experiment were performed using two 64 channel, PSI ESP64HD  $\pm 5$  kPa differential-pressure modules connected to a DTC Initium data acquisition system. Pressure was measured at the same scale-relative positions on the scaled FR8-LAB as the full-scale (Figure 28, Figure 29). Each measurement had a duration of 30 seconds, and a sampling rate of 300 Hz.

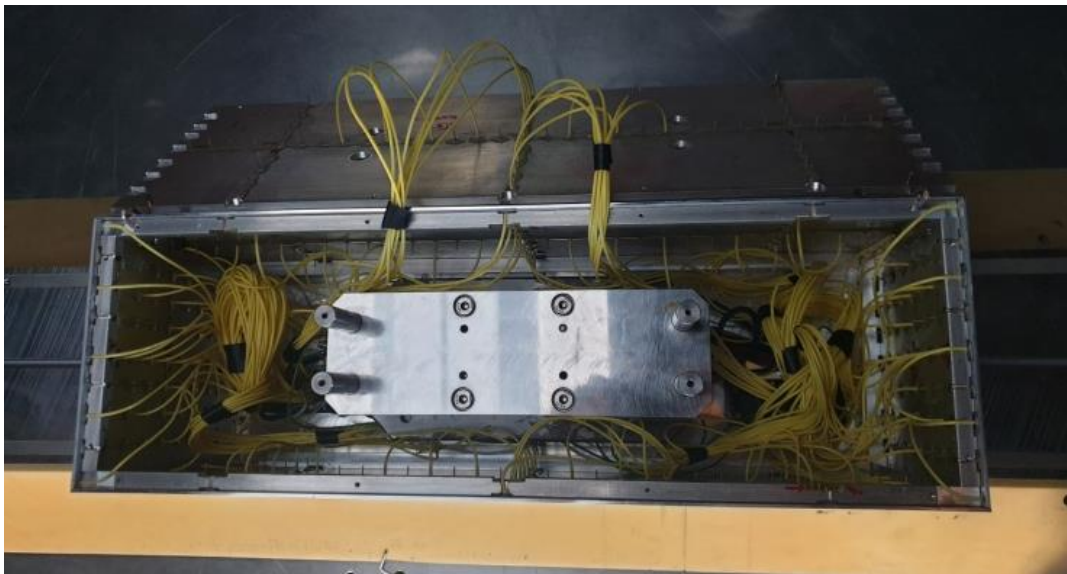


Figure 28: Surface Pressure measurement in Wind-tunnel experiment

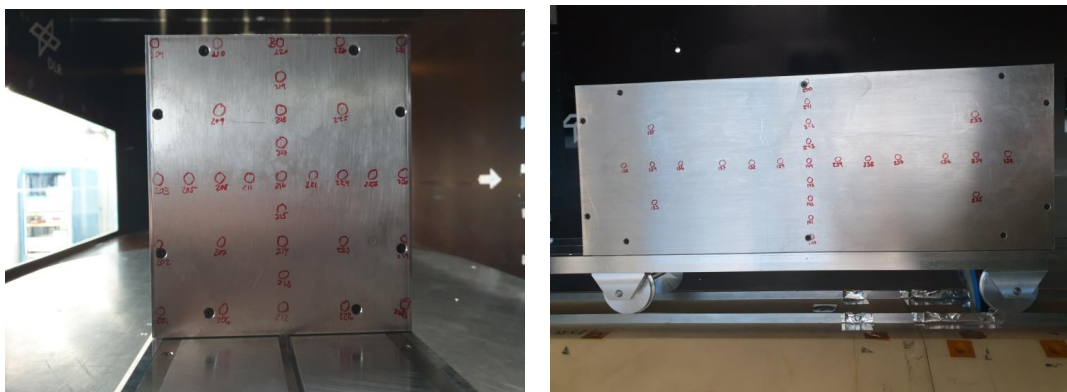


Figure 29: Pressure measurement locations on the scaled FR8-LAB wind-tunnel model

## Flow Visualization

The way in which air moves around the FR8-LAB is visualized using smoke injected by a 'smoke-wand' at specific points around the model in the reduced-scale wind-tunnel experiment. The visualization of the flow topology provides insight and provides explanations for the causes of the specific local pressures that occur on the surface of the FR8-LAB at different yaw angles.

### 0° Yaw (no crosswind)

At 0° yaw, the flow impinges/stagnates on the front (windward facing) surface - which corresponds to high pressure acting on the surface. The flow then moves outward, around the sides & over the roof, separating at the leading edges (Figure 30, Figure 31) and reattaching later - corresponding to lower pressure acting on the surface. Ahead of the front surface, above the wagon, the flow recirculates on itself (Figure 30, Figure 32). At the upper edge of the rear (leeward) surface, the flow separates and recirculates behind container, corresponding to low pressure acting on this surface (Figure 33).

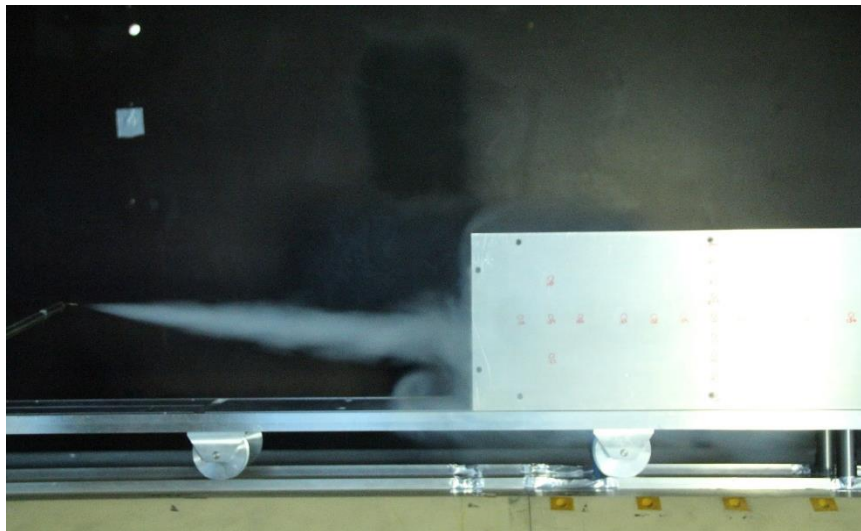


Figure 30: Smoke visualization over front windward surface (facing toward wind)

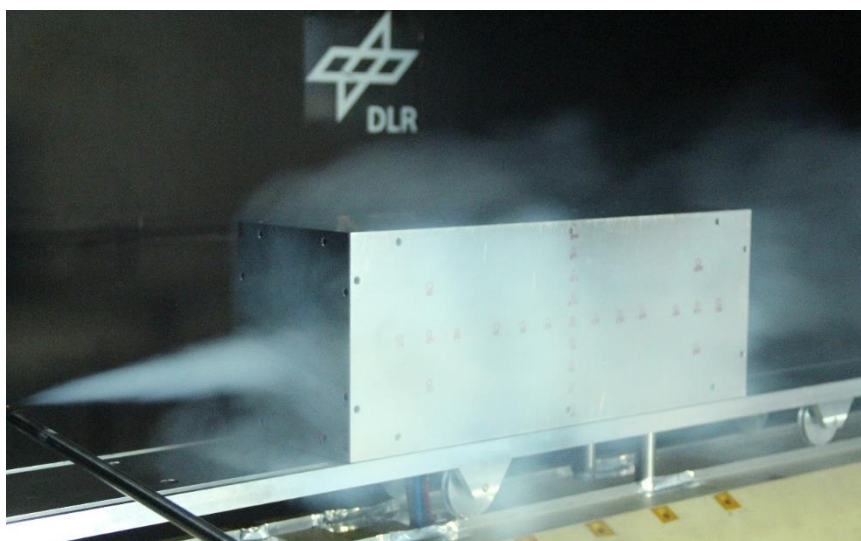


Figure 31: Smoke visualization over front windward surface (facing toward wind)



Figure 32: Highlighted smoke visualization over front windward (facing toward wind) surface

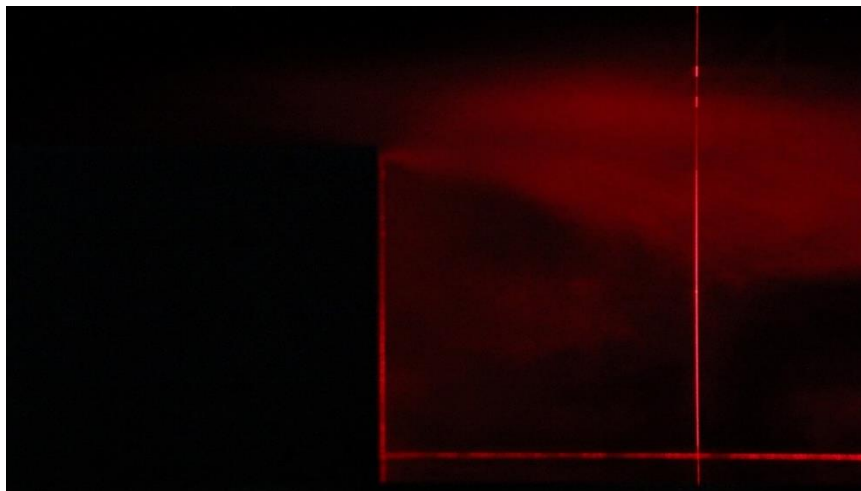


Figure 33: Highlighted smoke visualization over rear surface

### 10-60° Yaw (crosswind)

At moderate crosswind angles of 10-60°, the flow around the FR8-LAB has exhibits different characteristics, corresponding to different surface pressure characteristics. On the front and windward-side surface (the side facing towards the oncoming wind), the flow impinges / stagnates, again corresponding to high surface pressure. The flow moves over the container, separating from at the leading windward edge, forming a 3D longitudinal vortex (Figure 34, Figure 35), that would correspond to lower surface pressure. At the upper edge of the leeward side (the side facing away from the oncoming wind, effectively shielded from the wind by the rest of the body of the FR8-LAB), the flow separates and recirculates behind container, similar to the rear, again corresponding to low surface pressure.

### 15° Yaw (crosswind)

At even relatively small angles of crosswind, the flow that the FR8-LAB experiences is 'clean', not affected by upstream locomotive/container (Figure 36). This occurs when there is enough distance in front and enough crosswind (yaw angles > 15°).

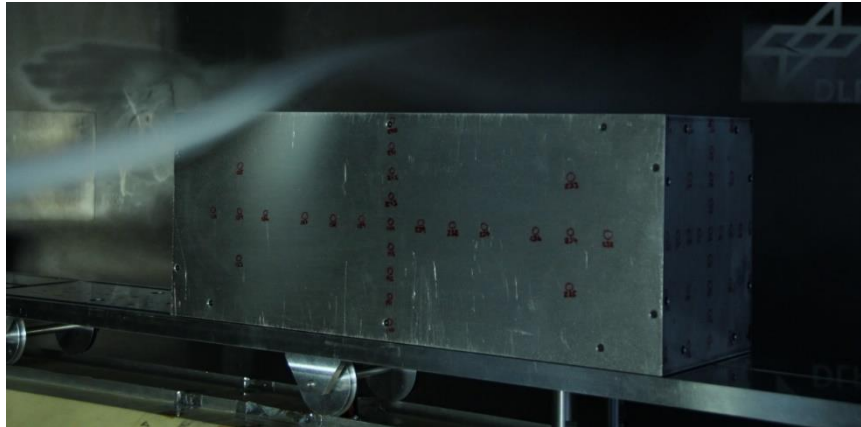


Figure 34: Smoke visualization over windward side (facing toward wind) during crosswind

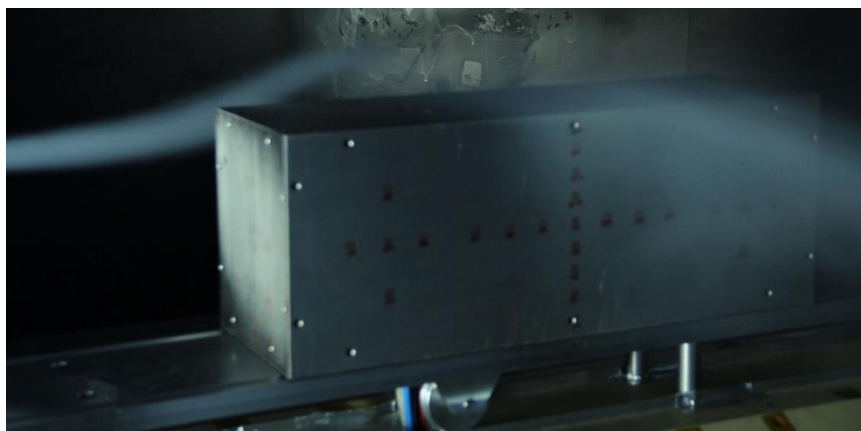


Figure 35: Smoke visualization over leeward side (shielded from wind) during crosswind

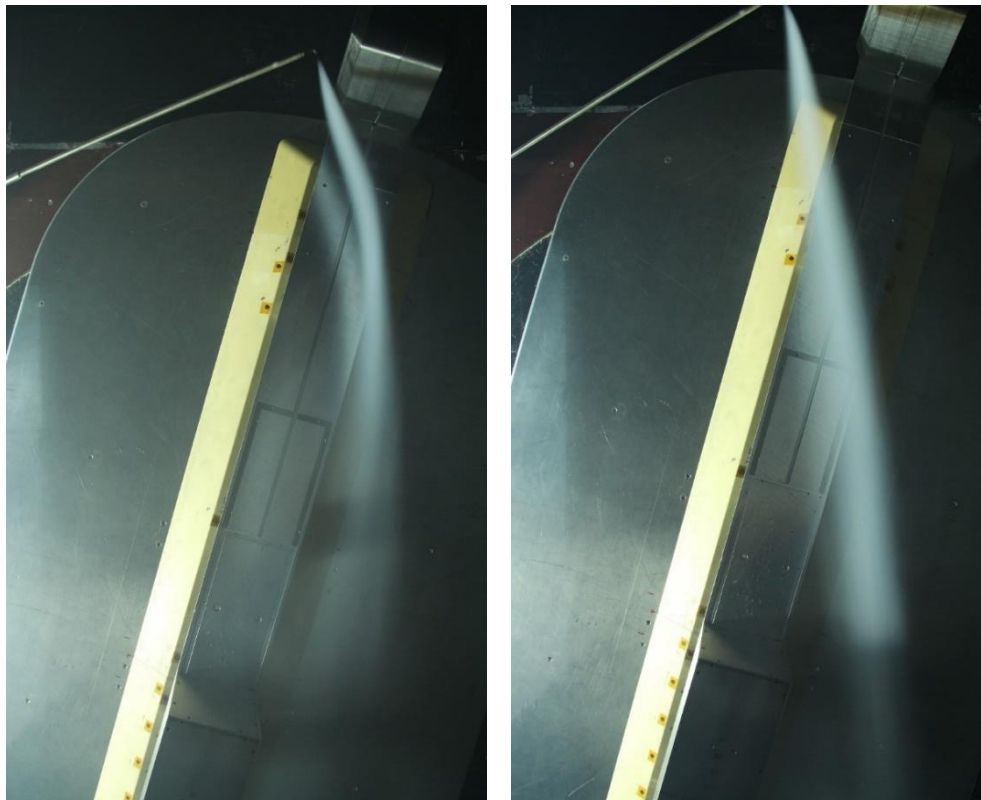


Figure 36: Smoke visualization top view: flow between upstream locomotive and downstream container

## Calibration Methodology

The methodology of combining the pressures at different surfaces to develop a calibration function, that is subsequently used to derive velocity, is outlined in this section.

### Pressure Characteristics

The calibration requires surface pressures that are sensitive to the yaw angle, in order to use that change in pressure to derive the yaw angle. The pressure at different surfaces (front, sides, rear and roof, as illustrated in Figure 37) over a yaw angles of 0-90° are presented in Figure 38. Pressure at the front, and left side (in this case, wind-ward side) show high sensitivity to yaw angle, with almost linear increase/decrease in pressure at these surfaces with increasing yaw angle. In contrast, the right (lee-ward side) and rear show far less sensitivity to changing yaw angle. The roof has a distinct decrease in pressure at 30-40°, but otherwise remains relatively low. These characteristics fit with the insight and explanations provided from the flow visualizations, in terms of high, low pressure being caused by stagnated flow and separation/recirculation respectively.

Crosses - made up of 9 pressure taps - in the center of each of the respective surfaces are illustrated in Figure 37. These were decided to be used as representative of the center of each of the surfaces, rather than relying on a single pressure sensor on each surface. This enables more robust measurements to be made in full-scale, where the average of 9 possible sensors can be used, and any erroneous sensors be disregarded. The effect of using the 9-sensor-cross is negligible compared to using a single centered sensor. This is demonstrated in Figure 38, where the solid line represents the 9-sensor cross and dotted line represents the single centered sensor – the respective pressure characteristics are the same.

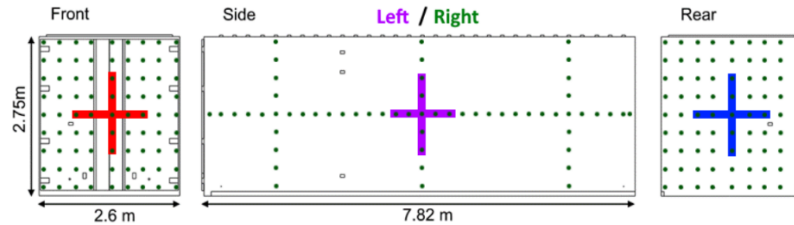


Figure 37: Pressure calibration surfaces

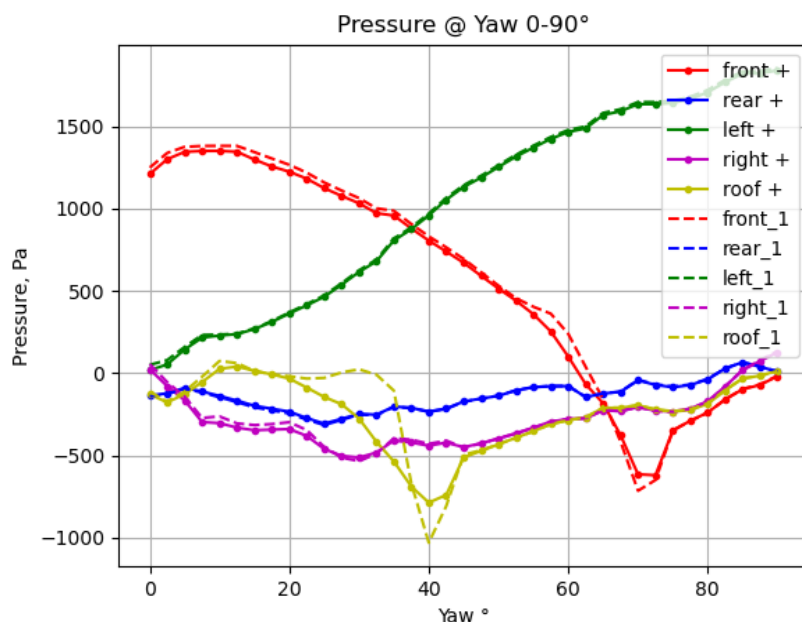


Figure 38: Pressure at each calibration surface for different static yaw angles

### Determination of Magnitude

The yaw angle the FR8-LAB is exposed to could potentially be determined simply from the pressure on the left and right sides. However, the magnitude of the wind the FR8-LAB is exposed to would be unknown. To derive this, a combination of the surface pressures is used to provide something analogous to 'dynamic pressure',  $Q_R$ , which can be used to determine the magnitude of the velocity of the airflow in the wind tunnel, or wind the FR8-LAB is exposed to in operation. The dynamic pressure is the total pressure, minus the static pressure in the flow-field. Considering the exposure of the FR8-LAB to yawed flow (experiencing flow on the front, and windward surfaces), and the different pressure variation over yaw angles in Figure 38, a relationship between the different surface pressures was developed to estimate the dynamic pressure in the flow field:

- $Q_R = \sqrt{((p_{\text{front}} - p_{\text{rear}})^2 + (p_{\text{left}} - p_{\text{right}})^2)}$

where  $p_{\text{front}}$ ,  $p_{\text{rear}}$ ,  $p_{\text{left}}$ ,  $p_{\text{right}}$  are the average pressures from the 9-sensor cross at each respective surface.

This 'resultant' dynamic pressure,  $Q_R$  (solid black line) compares well to the dynamic pressure,  $Q$ , measured directly in the wind-tunnel experiment with a Pitot-static tube in the test-section (dotted black line), as illustrated in Figure 39.

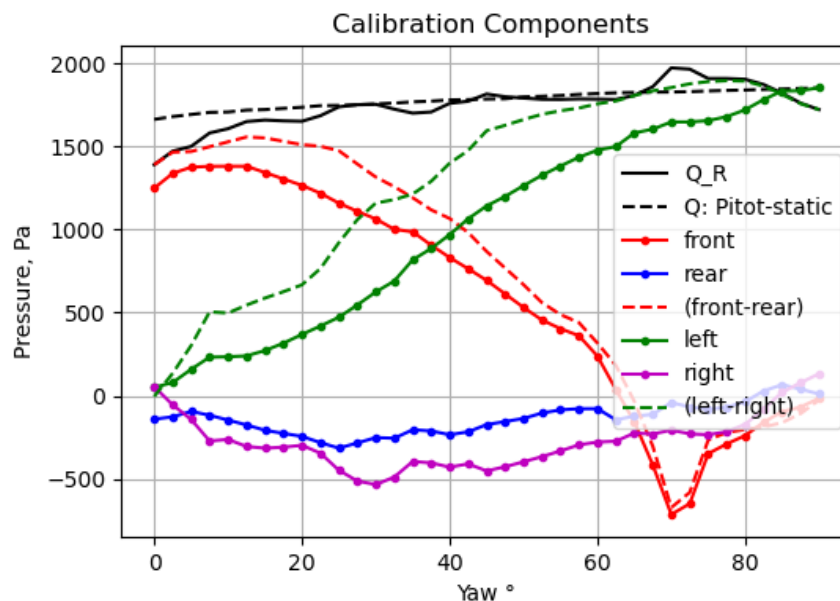


Figure 39: Calibration components

The resultant dynamic pressure,  $Q_R$ , can be used to normalize the measured pressure at each surface: Normalized pressure = Pressure/ $Q_R$  (Figure 40). This demonstrates the suitability of  $Q_R$  as an estimator of real  $Q$ , the  $P/Q_R$  of ~1 at front & rear during yaw angle variation are consistent with typical yawed bluff-body pressure distribution.

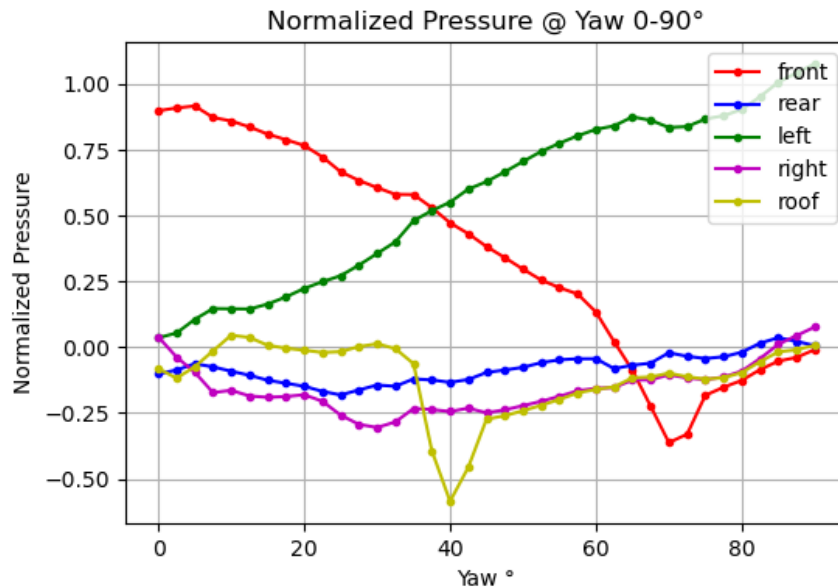


Figure 40: Normalized Pressure at different static yaw angles

With the magnitude of the wind the FR8-LAB is exposed to being estimated, the angle can now be derived from the pressure. This is determined, by assessing the pressure differential between either side of the FR8-LAB, and using the dynamic pressure to normalize to develop a calibration coefficient:

- **Calibration coefficient =  $(p_{\text{left}} - p_{\text{right}}) / Q_R$**

where  $p_{\text{left}}$ ,  $p_{\text{right}}$  are the average pressures from the 9-sensor cross at each respective side surface.

This concept of using surface pressures at different locations on the FR8-LAB is a similar concept as 'train/car-as-probe' in vehicle aerodynamics, and dynamic-pressure multi-hole probes (used as wind-tunnel measurement devices) utilized previously in applied aerodynamic research. The variation of the calibration coefficient with yaw angle is illustrated in Figure 41. There is now a defined relationship between surface pressures on the FR8-LAB (combined into the calibration coefficient) and the yaw angle the FR8-LAB is exposed to.

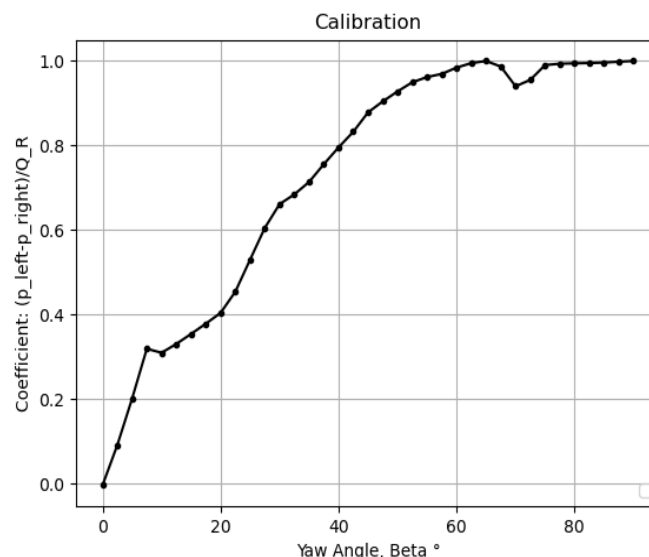


Figure 41: Calibration Coefficient

## Calibration Robustness

The robustness of the calibration coefficient profile was investigated through repeatability tests, and sensitivity to Reynolds Number, loading configuration and freestream turbulence intensity. In Figure 42, the calibration is demonstrated to be repeatable, and largely insensitive to differences in the Reynolds number and turbulence intensity tested at. Only minor sensitivity is visible at  $\sim 10^\circ$  yaw angle, which would correspond to relatively low crosswinds, thus not the primary focus of this investigation. The calibration shows greater sensitivity to loading configuration; as one would expect, the closer an upstream object (other container or locomotive) is the FR8-LAB, the more it shields it from flow at low yaw angles, affecting the magnitude of pressure acting on the forward-facing surface, thereby affecting the calibration coefficient. However, even at the smallest gap tested in full-scale of 9.3m (corresponding to the 'small gap' labelled in Figure 42), beyond  $30^\circ$  degrees yaw, the calibration is consistent across all loading configurations, and for a gap of 17.8m (corresponding to the 'large gap' labelled in Figure 42), consistent from  $20^\circ$  degrees yaw. Based on these results, the standard calibration profile was applied to all measurements, and assessed for data sanity, for overall simplicity of the processing and interpretation of the results. However, for future similar investigations, particularly without the specific test-wagon configuration utilized in this investigation with considerably large gaps either side of the FR8-LAB, a calibration profile that is dependent on the loading configuration could be developed if needed.

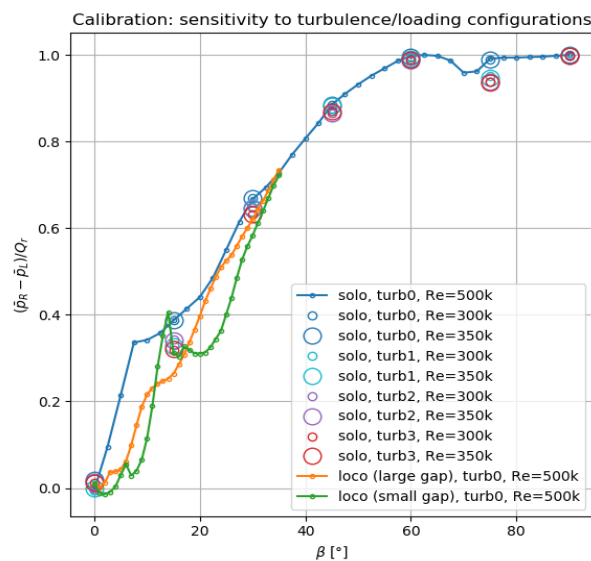


Figure 42: Calibration sensitivity

## Application of Calibration

Utilizing the calibration profile, the surface pressures on the FR8-LAB in operation could be processed to derive the velocity components magnitudes and angle:

- **V<sub>R</sub>**: resultant wind train experiences – from pressure combination:  $Q_R$  and  $Q=0.5 \cdot \text{density} \cdot V^2$ , therefore  $V_R = \sqrt{2 \cdot Q_R / \text{density}}$  where density is obtained from the local weather station
- **$\beta$** : relative angle of wind that train experiences – from wind-tunnel calibration

The airflow the FR8-LAB experiences due to its movement, has the same magnitude of the train speed, just in the opposite direction:

- **V<sub>T</sub>**: train-speed induced-flow - from satellite navigation system, GNSS

The atmospheric wind, that the FR8-LAB is exposed to (in addition to the flow generated by movement of the train):

- **V\_W**: atmospheric wind (result to infer/find)

Can be determined using vector addition (illustrated in Figure 43), processing the known/measured  $V_R$  and  $V_T$ , to determine  $V_W$ :

- **$V_R = V_T + V_W$**   
therefore,
- **$V_W = V_R - V_T$**

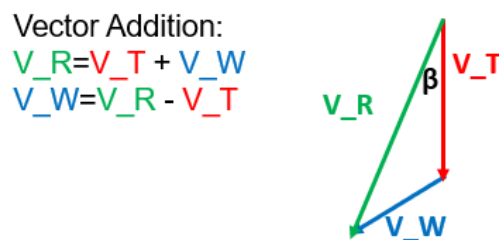


Figure 43: Vector addition of different velocity components acting on the FR8-LAB during motion and exposure to crosswind

## Results

### System Functionality

The functionality of the FR8-LAB measurement system is demonstrated in this section. The train speed, topography distances measured by the LiDAR sensors, and transient pressure at different locations during a typical bridge-crossing measurement are presented in Figure 44. In this figure, and those following, the ends of the tunnel are denoted as vertical solid black lines, and the ends of the bridge as vertical dotted lines.

The example measurement presented is with relatively high crosswind. From the start of the measurement displayed, the train accelerates, and then remains mostly constant, with only minor accelerations/decelerations before and after the bridge. The LiDAR measurements on the sides and roof clearly identify operation through the tunnel, where the measured distance at each position from the FR8-LAB surface to the wall/roof of the tunnel is ~2.7m. Beyond the tunnel, the LiDAR identifies mostly open-air operation (no large, noticeable infrastructure/topography in close proximity to the FR8-LAB).

The transient pressure shows clear increase at the front of the train, and decrease in pressure over the sides, roof and rear, as the train accelerates (Figure 44 c). After an initial peak as the train enters the tunnel, the pressure is relatively constant, before decreasing in magnitude after exiting the tunnel. As the FR8-LAB starts to cross the bridge, being exposed to the crosswind, the pressure at the front increases, as well as the left side, in this case being the wind-ward side. Conversely, the right side (leeward), rear and roof exhibit a decrease in pressure. Clear, coherent pressure fluctuations of magnitudes up to 100 Pascals (Pa) are also visible as the FR8-LAB is exposed to the crosswind, particularly on the front, both sides and roof, whilst the rear is more stable. After exiting the bridge, the pressure on the windward side reduces back to similar levels as the leeward side and rear, and there are no longer significant, large-scale pressure fluctuations.

In Figure 45 and Figure 46, the transient pressure of a high crosswind ( $\sim 12\text{m/s}$ ) and low crosswind ( $\sim 4\text{m/s}$ ) bridge-crossing measurement are presented respectively. For the high crosswind example, clear fluctuations of over 100 Pa are visible with high pressure on front and windward side, with low pressure on the lee-ward side, rear and roof. In contrast, the low crosswind example, only high pressure, with medium, small-scale fluctuations occur on the front surface, with the rear, sides, roof exhibiting minimal pressure or fluctuations.

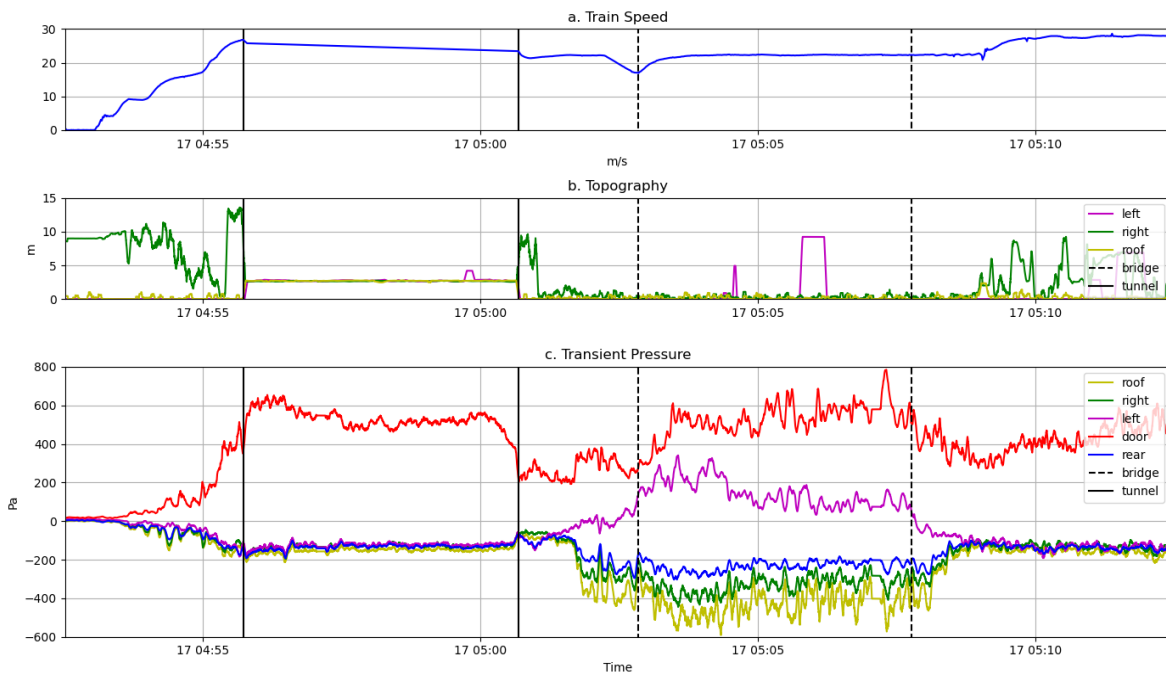


Figure 44: Measurements demonstrating system functionality during bridge-crossing: a. Train speed., b. LiDAR distance measurements, c. transient pressure

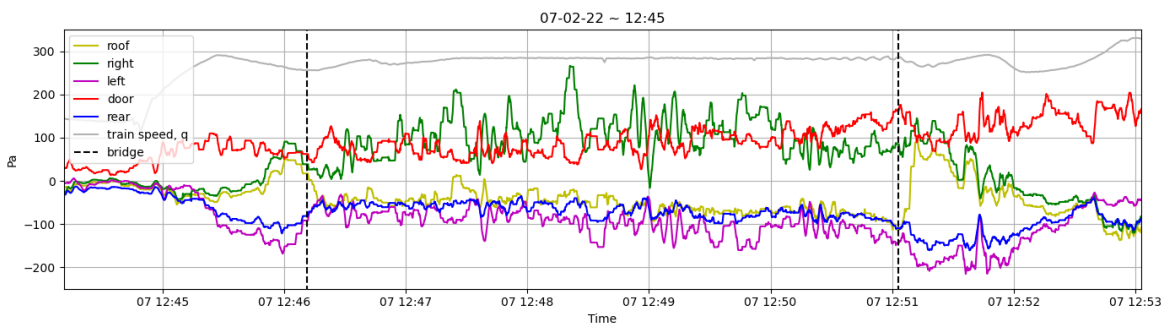


Figure 45: Transient pressure during relatively high crosswind exposure

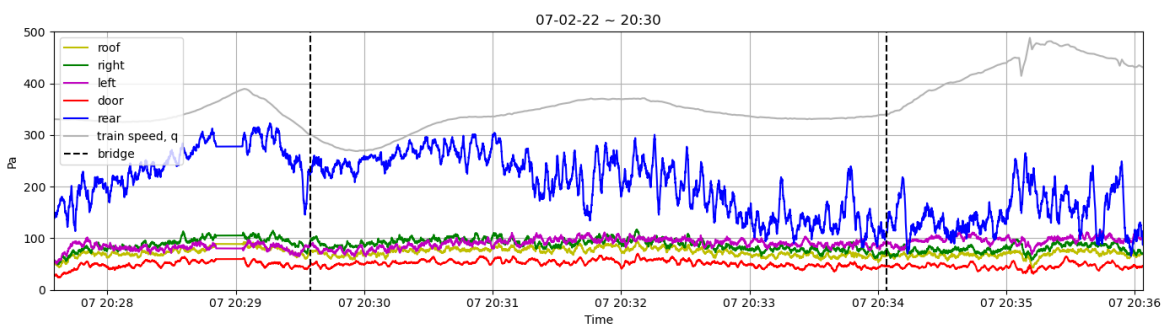


Figure 46: Transient pressure during relatively low crosswind exposure

## Calibration Example

The average transient pressure of 9 sensors in a cross formation on the front, rear, left and right sides, referred to as 'calibration surfaces' are presented in Figure 47 for an example bridge-crossing measurement. These results are then converted to a resultant dynamic pressure,  $Q_R$  (Figure 48), calibration coefficient (Figure 49) and yaw angle (Figure 50), using the process outlined above.

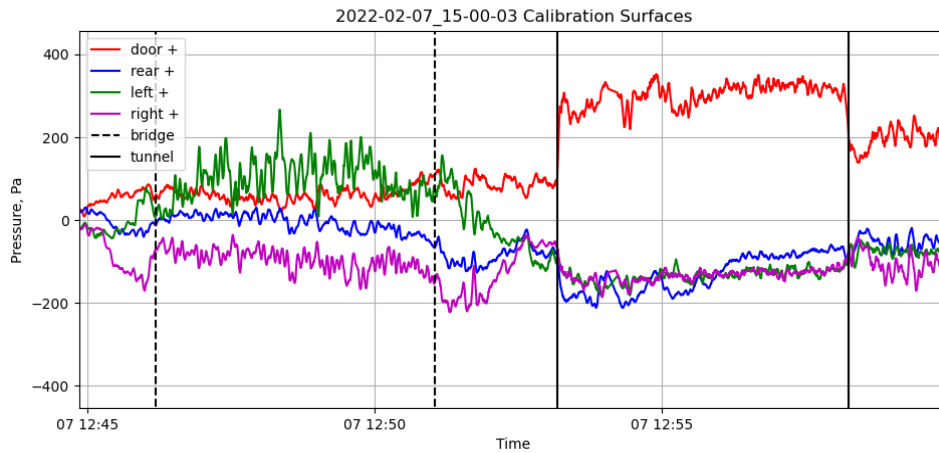


Figure 47: Transient pressure at each of the calibration surfaces during bridge-crossing and tunnel entry/exit

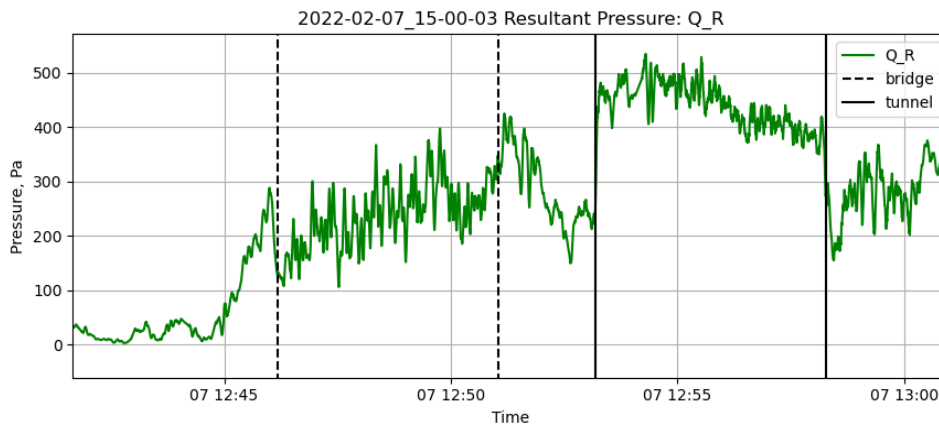


Figure 48: Resultant dynamic pressure,  $Q_R$  during bridge-crossing and tunnel entry/exit

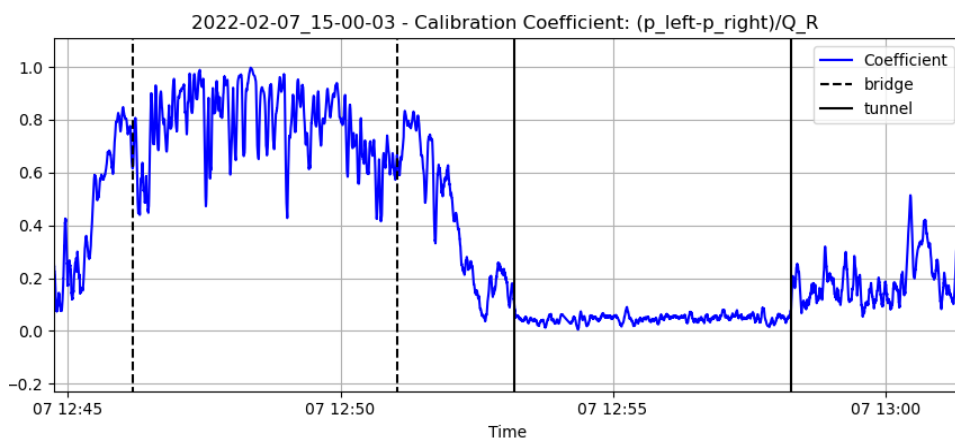


Figure 49: Calibration Coefficient during bridge-crossing and tunnel entry/exit

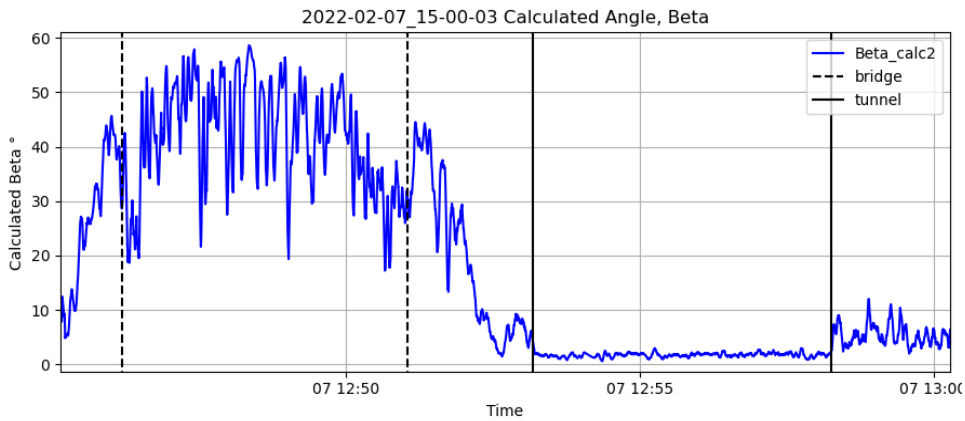


Figure 50: Derived Yaw angle Beta during bridge-crossing and tunnel entry/exit

The 'resultant' dynamic pressure,  $Q_R$  is then converted to the resultant velocity,  $V_R$  and with vector addition ( $V_R = V_T + V_W$ ), the train speed induced wind  $V_T$  (determined from the GNSS), and atmospheric wind  $V_W$  are derived. All three velocity components are presented for the same example bridge-crossing measurement in Figure 51, with representative mean and instantaneous vectors illustrated in Figure 52.

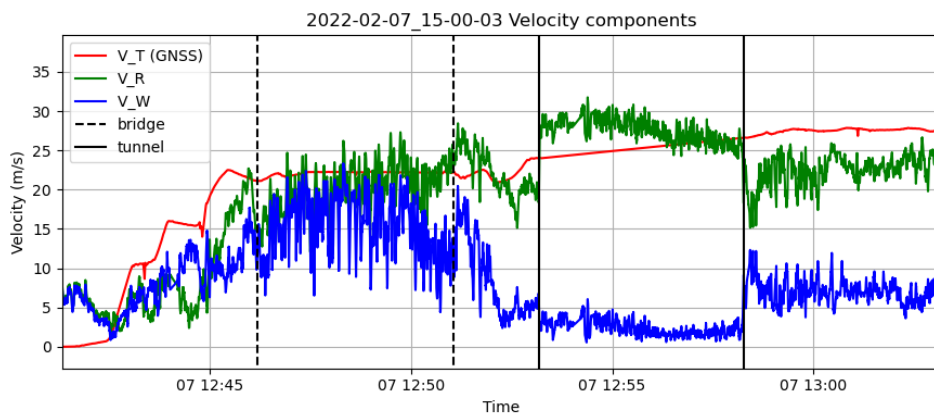


Figure 51: Velocity components  $V_T$ ,  $V_R$  and  $V_W$ , during bridge-crossing and tunnel entry/exit

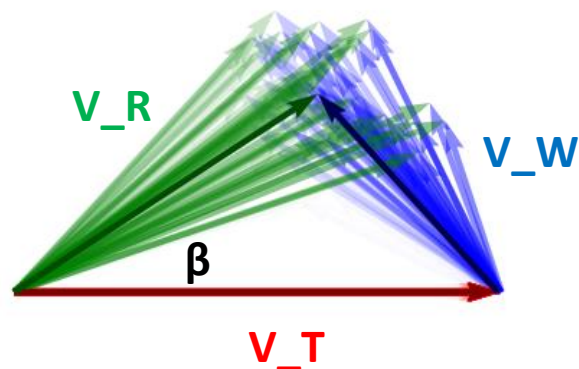


Figure 52: Velocity component vectors during bridge-crossing, mean: dark lines, different instantaneous: individual semi-transparent lines

## Validation

In this section, the velocities derived from the surface pressure measurements on the FR8-LAB, utilizing the process as outlined in the above section, are compared against the DB ST ultrasonic anemometers (USA1 and USA2) as well as the available weather station data.

In interpreting these results, it should be noted the USA's are purpose-built devices for measuring wind velocity, in contrast to the novel measurement technique and processing required to derive velocity using the FR8-LAB. In addition, there was 9 m spacing between USA1 and USA2, with corresponding distances of 36 and 45 m of the USAs to the FR8-LAB. Further, the ambient wind that a moving freight-train is exposed to is turbulent with non-negligible spatial and temporal fluctuations.

The movement of the train through air, represents a velocity component that velocity measurement equipment like the USAs and FR8-LAB would measure even with no crosswind present – this is denoted as  $V_T$ , and referred to as train speed. In the presence of a crosswind in the atmosphere,  $V_W$ , the measurement devices on the test-wagon consist measure the resultant,  $V_R$ , of both the train speed, and the atmospheric crosswind  $V_W$ . Thus,  $V_R = V_T + V_W$ ; considering the velocity components as vectors, where each have respective magnitudes and directions.

In Figure 53, the resultant velocity,  $V_R$  (the total velocity the probes would measure on the train) are presented for a specific, relatively high crosswind measurement across the bridge. The USAs 1 & 2 and the FR8-LAB results are presented both with a one second moving-average applied (1s), as well as a 60 second moving-average. Comparison of the different measurement shows strong agreement in both the long-term trend visible in the 60s profiles, as well as the temporal fluctuations visible in the 1s profiles. The same measurements are presented in Figure 54 also including either side of the bridge crossing. This further demonstrates the similarity between the USAs and the FR8-LAB velocity results, even in different operating scenarios beyond the bridge. It should be noted however, that the FR8-LAB is calibrated for relatively open-air operation, such as the bridge. This is the configuration that was modelled in the wind-tunnel. In different operating conditions, such as a tunnel, the pressure characteristics could be different, and exhibit different sensitivities to yaw angle. Therefore, the FR8-LAB derived velocities during the tunnel in particular are not robust (in any case there are no USA results to compare directly to).

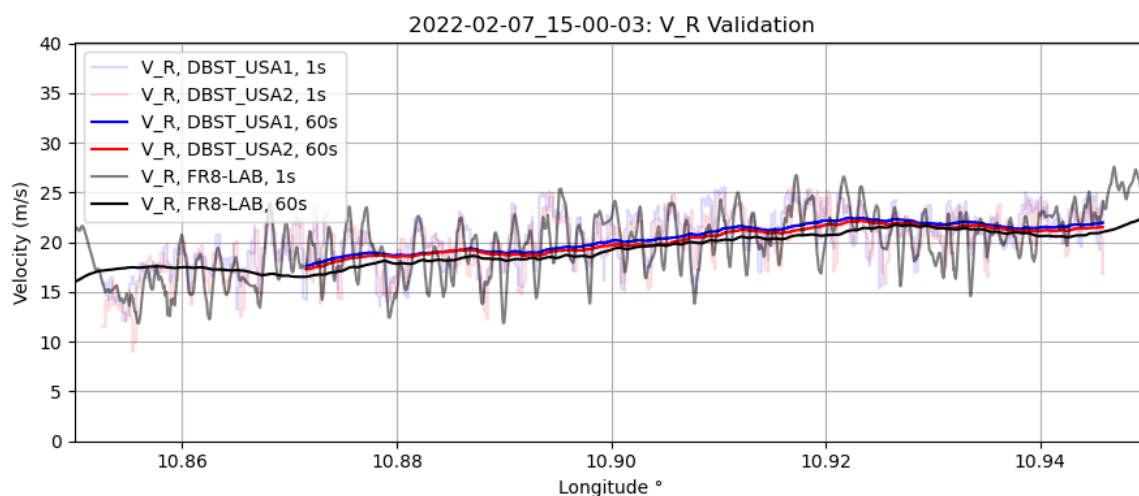


Figure 53: Resultant velocity  $V_R$  derived by the FR8-LAB, and measured by the DB ST Ultrasonic Anemometers USA1, USA2 during the same bridge-crossing

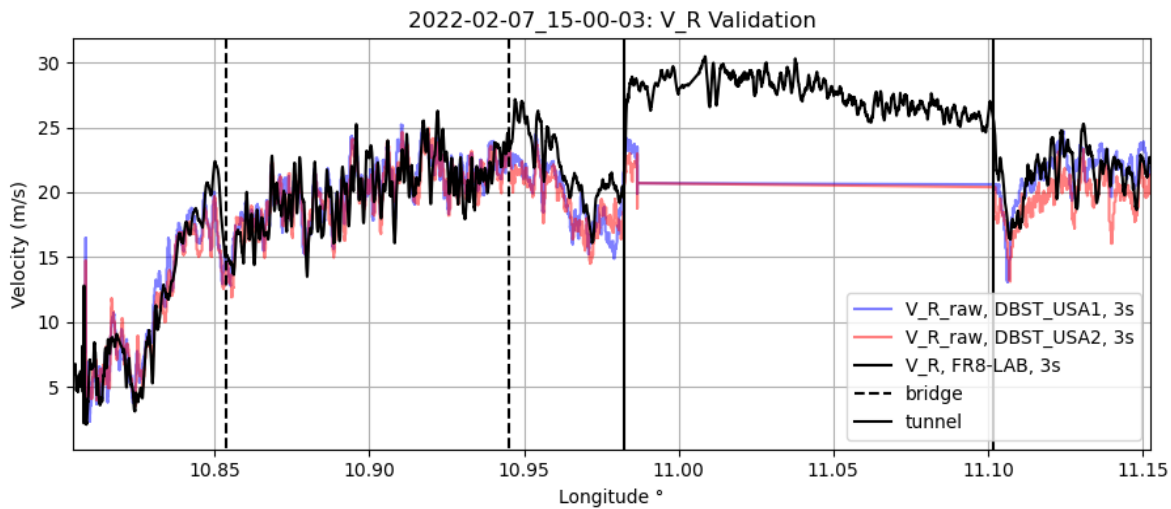


Figure 54: Resultant velocity  $V_R$  derived by the FR8-LAB, and measured by the DB ST Ultrasonic Anemometers USA1, USA2 during the bridge crossing, tunnel entry/exit and either side of each on land

In Figure 55, the atmospheric wind component,  $V_W$ , of the velocity measured by both the USAs and FR8-LAB (i.e. the velocity measured by the equipment, with the train speed component removed) is presented for the same specific bridge crossing as in Figure 53. Again, the velocities of the USAs and FR8-LAB exhibit strong agreement, in the long-term profiles (60s) and short-term fluctuations (1s profiles). Similarly, in Figure 56, Figure 57, Figure 58, three other specific bridge crossings are presented showing strong agreement between the USAs and the FR8-LAB derived velocity. The different bridge crossings presented all have crosswind present, but occur at different days, with different magnitudes, and different time-varying characteristics like long-term and short-term fluctuations. Of course, there exists some differences between the FR8-LAB derived velocity and the USA measured velocities (there are visible differences even between the two USAs) but some variation is to be expected due to the different measurement positions of the equipment, the turbulent nature of the wind that has temporal and spatial fluctuations of different scales, as well as the different manner in which the velocity is determined between the USAs and the FR8-LAB.

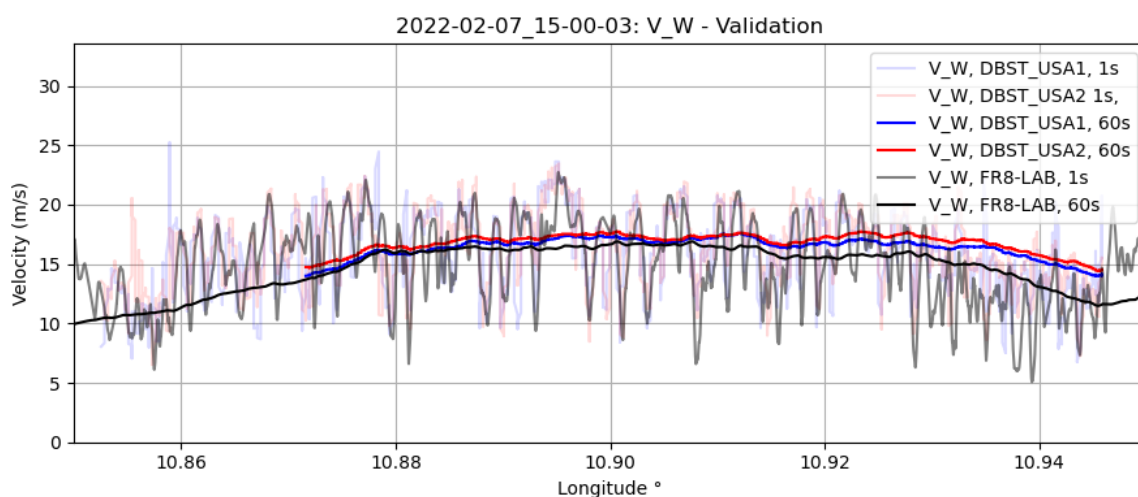


Figure 55: Wind velocity  $V_W$  derived by the FR8-LAB, and measured by the DB ST Ultrasonic Anemometers USA1, USA2 during the same bridge-crossing, example 1

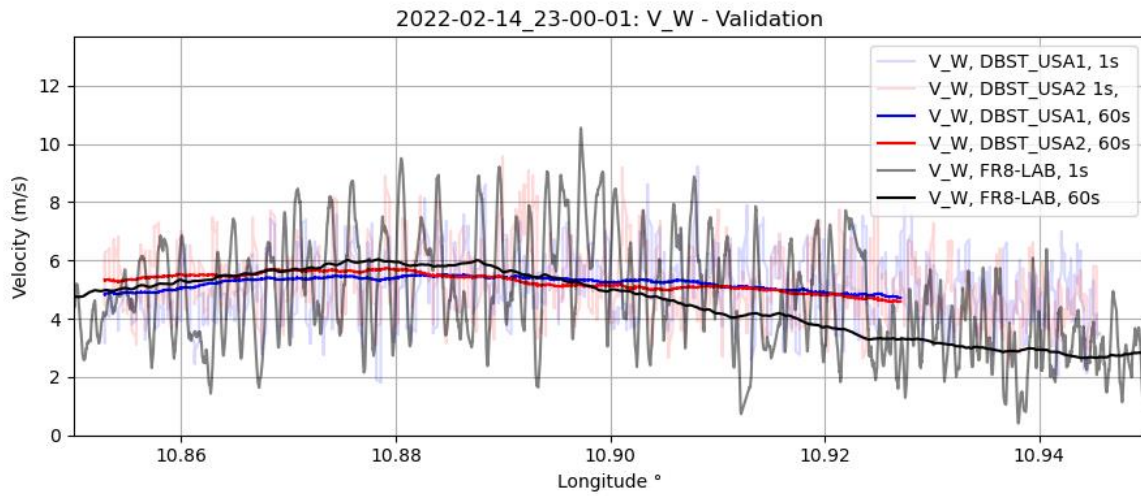


Figure 56: Wind velocity  $V_W$  derived by the FR8-LAB, and measured by the DB ST Ultrasonic Anemometers USA1, USA2 during the same bridge-crossing, example 2

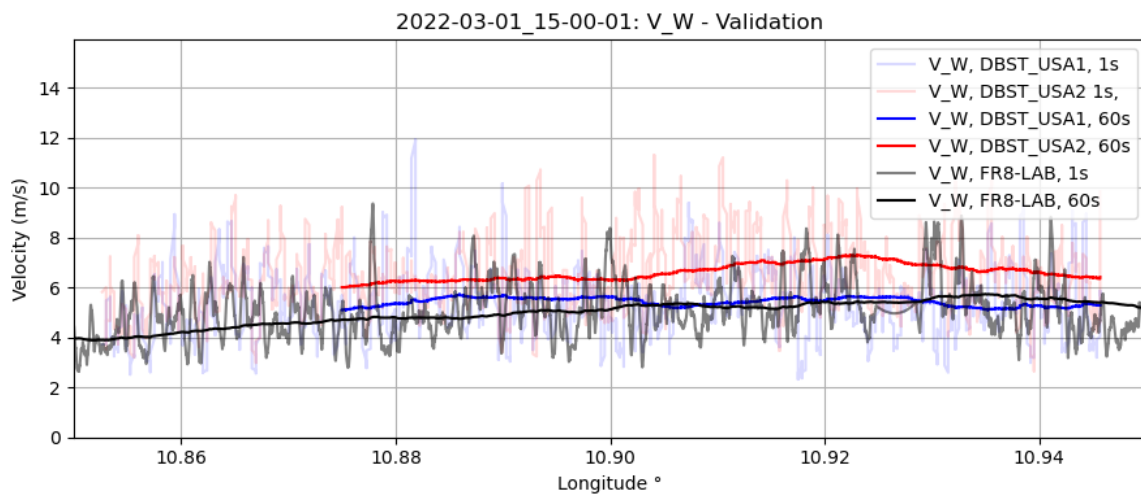


Figure 57: Wind velocity  $V_W$  derived by the FR8-LAB, and measured by the DB ST Ultrasonic Anemometers USA1, USA2 during the same bridge-crossing, example 3

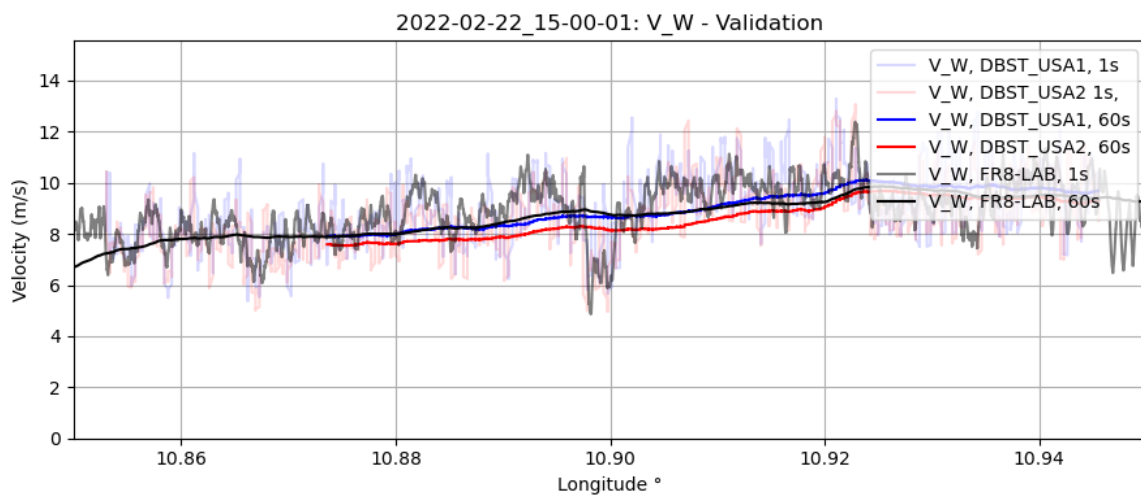


Figure 58: Wind velocity  $V_W$  derived by the FR8-LAB, and measured by the DB ST Ultrasonic Anemometers USA1, USA2 during the same bridge-crossing, example 4

In addition to the DB ST USAs, weather data was obtained as an alternative source for validation of the DLR FR8-LAB derived velocity results. The most appropriate weather station data available - from the weather station on the island of Omø in the same body of water (as described above) - is compared to the USAs and FR8-LAB measurements in Figure 59. In this figure, the USA and FR8-LAB results are presented with 3s moving-averages to directly compare to the largest 3s gust data available from the weather station, in addition to the 10min mean. The mean velocity of the weather station is comparable to the average velocity of the USAs and the FR8-LAB, validating the general magnitude measured by the equipment on the train. The 3s peak of the weather station is less comparable to the peak 3s profiles of the USAs and FR8-LAB. However, even with 3s moving-average applied, these peaks can be expected to be more localized to the bridge area, thus less likely to perfectly compare to Omø as the nearest available weather station.

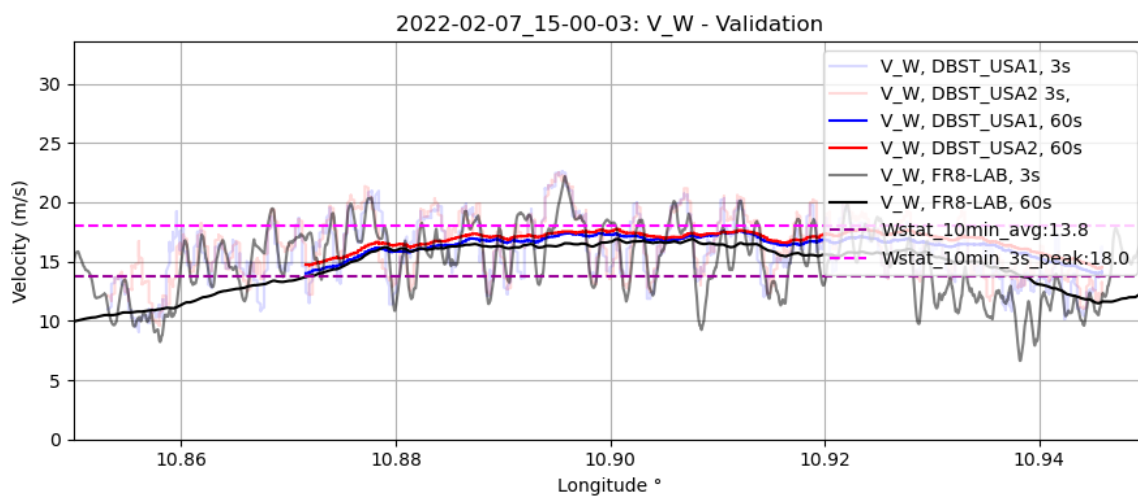


Figure 59 Wind velocity  $V_W$  derived by the FR8-LAB, and measured by the DB ST Ultrasonic Anemometers USA1, USA2 during the same bridge-crossing, compared to best available weather station data (Omø) during 10min window at the time of the bridge-crossing.

## Time-Varying Crosswind

### Individual Insight

Analysis of the time-varying crosswind characteristics of specific bridge crossing measurements are presented in this section. This provides an idea of what type of time-varying velocities are possible to be exposed to, during a bridge crossing.

In Figure 60, the time-varying velocities of a specific bridge crossing are presented. Profiles with moving averages (MA) of 0.1s, 3s, 6s and 10s are included, as well as the mean velocity across the entire bridge (typically corresponding to ~5minutes, but of course dependent on the train velocity), as well as across the center half of the bridge. In this figure, significant time-varying characteristics are visible, with multiple clear peaks in velocity, 'gusts', with magnitudes of 20m/s or more (depending on the moving-average duration) during the bridge crossing. In this example, it is clear that the mean is not a good representative of the actual velocity the train experiences at a given instant of time, due to the time-varying, fluctuating nature of the measured wind.

In Figure 61, the same specific bridge-crossing measurements are presented as in Figure 60, however with normalized velocity plotted. Here, the time-varying velocity is normalized - dividing the time-varying velocity with the mean velocity across the entire bridge - and presented as a percentage, %. In this way, the peak velocities above noted as having magnitudes of up to 20m/s, can be described as ~50% velocity peaks relative to the mean across the full-bridge.

Additionally included in Figure 61 (right), is the probability density of the normalized velocity fluctuations. This provides insight into the occurrence of the different velocity fluctuation magnitudes for the specific measurement analysed.

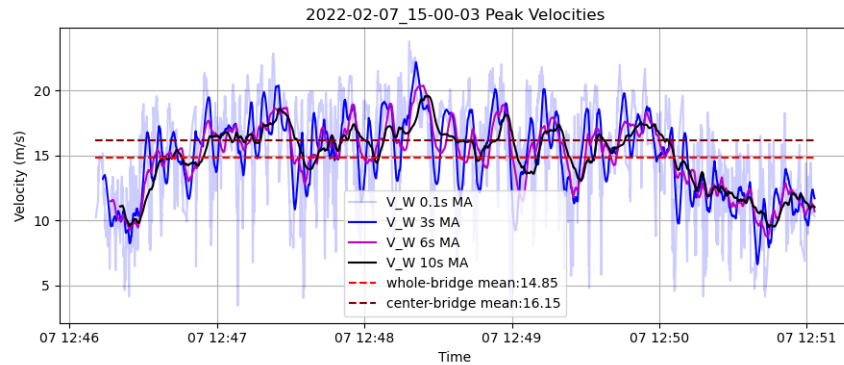


Figure 60: Time-varying velocity,  $V_W$ , specific example 1

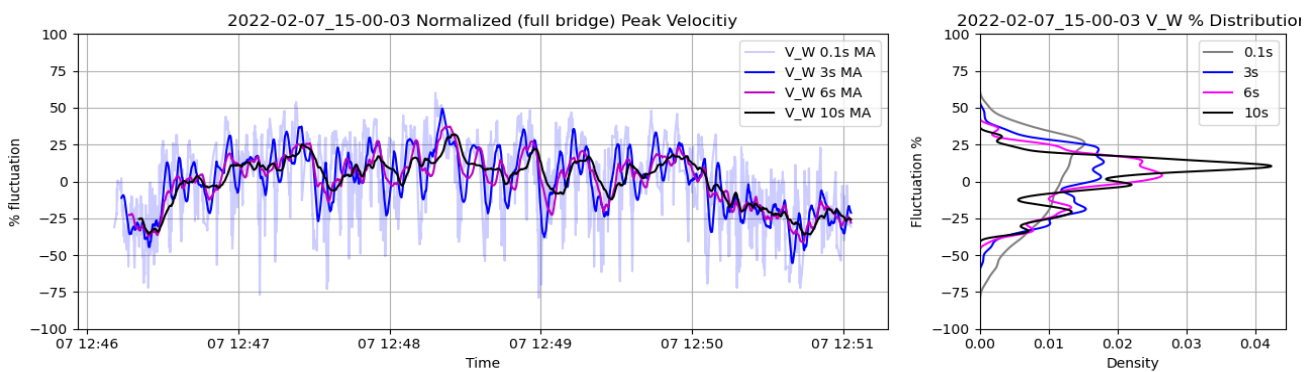


Figure 61: Normalized time-varying velocity,  $V_W$ , left, with corresponding probability density (right), example 1

Another three different specific bridge crossings during crosswind are presented in Figure 62 – Figure 68 (velocity, normalized velocity and the probability density). Further transient velocity figures during 30 bridge-crossings with mean crosswinds greater than 5 m/s are included in the Appendix. The four different bridge-crossing measurements exhibit different mean characteristics (5 to 16 m/s), fluctuation levels and probability density, and even long-term trends (peaking in the middle of the bridge, increasing gradually over time, relatively constant). Inspecting the normalized velocity enables a more direct comparison to be made between different measurements with different mean values. However, it is clear from these specific measurements presented, that the time-varying wind velocity exhibits significant fluctuation characteristics, but further, these characteristics themselves differ between individual bridge crossings.

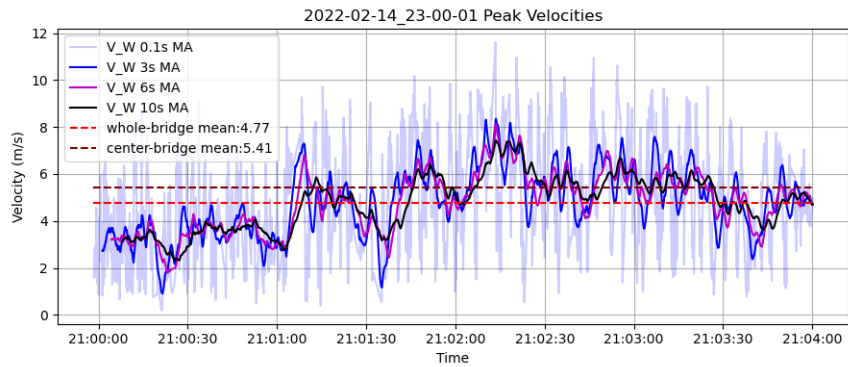


Figure 62: Time-varying velocity,  $V_W$ , specific example 2

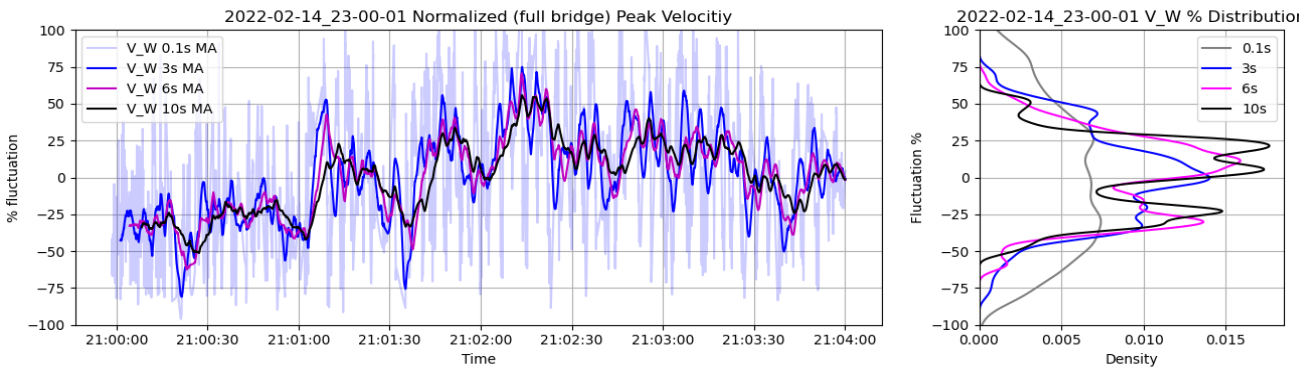


Figure 63: Normalized time-varying velocity,  $V_W$ , left, with corresponding probability density (right), example 2

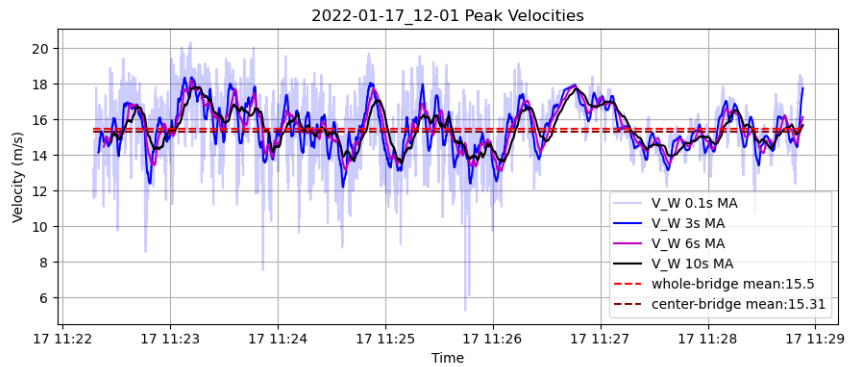


Figure 64: Time-varying velocity,  $V_W$ , specific example 3

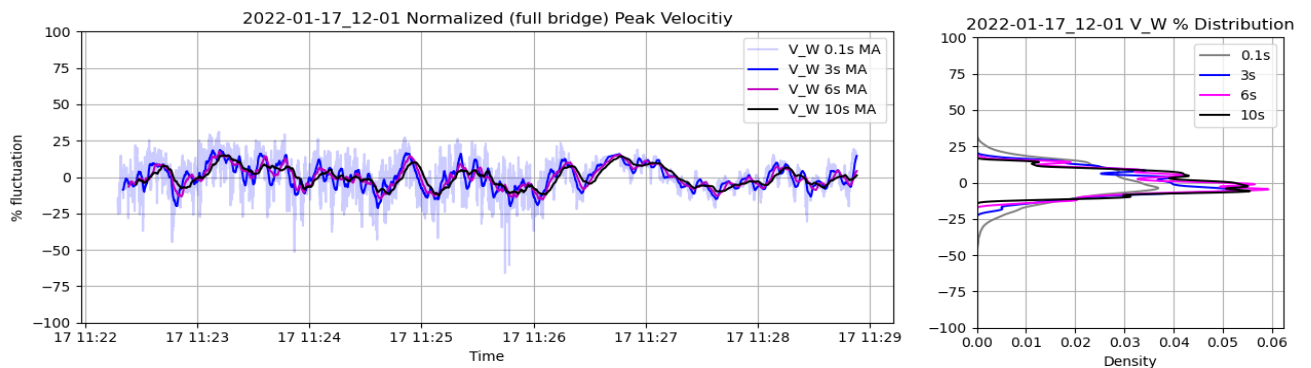


Figure 65: Figure 66: Normalized time-varying velocity,  $V_W$ , left, with corresponding probability density (right), example 3

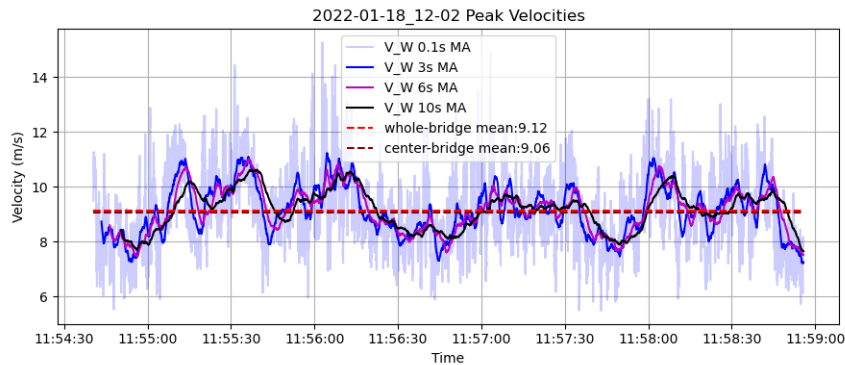


Figure 67: Time-varying velocity,  $V_W$ , specific example 4

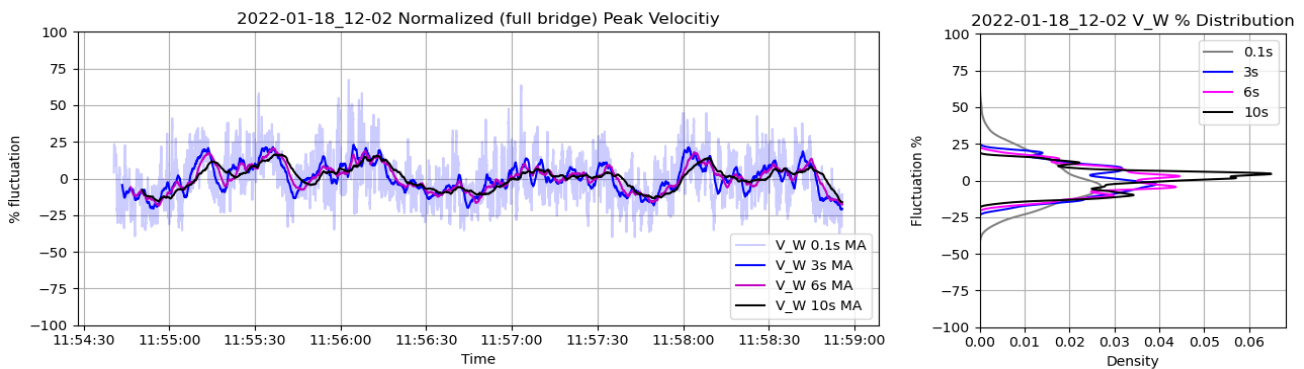


Figure 68: Figure 69: Normalized time-varying velocity,  $V_W$ , left, with corresponding probability density (right), example 4

### General Crosswind Characteristics

A general description of crosswind characteristics has been developed from the collation of multiple individual bridge-crossing measurements. All bridge crossings measurements where the mean crosswind was greater than 5m/s were normalized & collated (as illustrated in Figure 70). This resulted in 30 individual bridge-crossing measurements being processed. The normalisation of the velocity makes the data comparable, enabling the individual runs to be collated and processed together (the results are no longer specific to a particular mean wind speed at a given day).

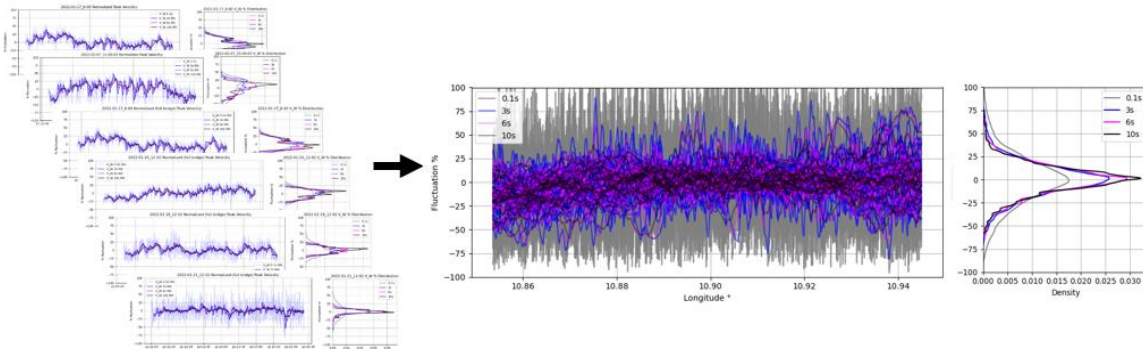


Figure 70: Normalized individual runs are collated together and processed to provide general crosswind characteristics.

The collated raw, normalized and probability density data are presented in Figure 71. The varying velocity ranges of the different individual measurements are visible in Figure 71 (upper), but once normalized in Figure 71 (lower) their relative similarity, and ability to be compared, collated and processed together is evident.

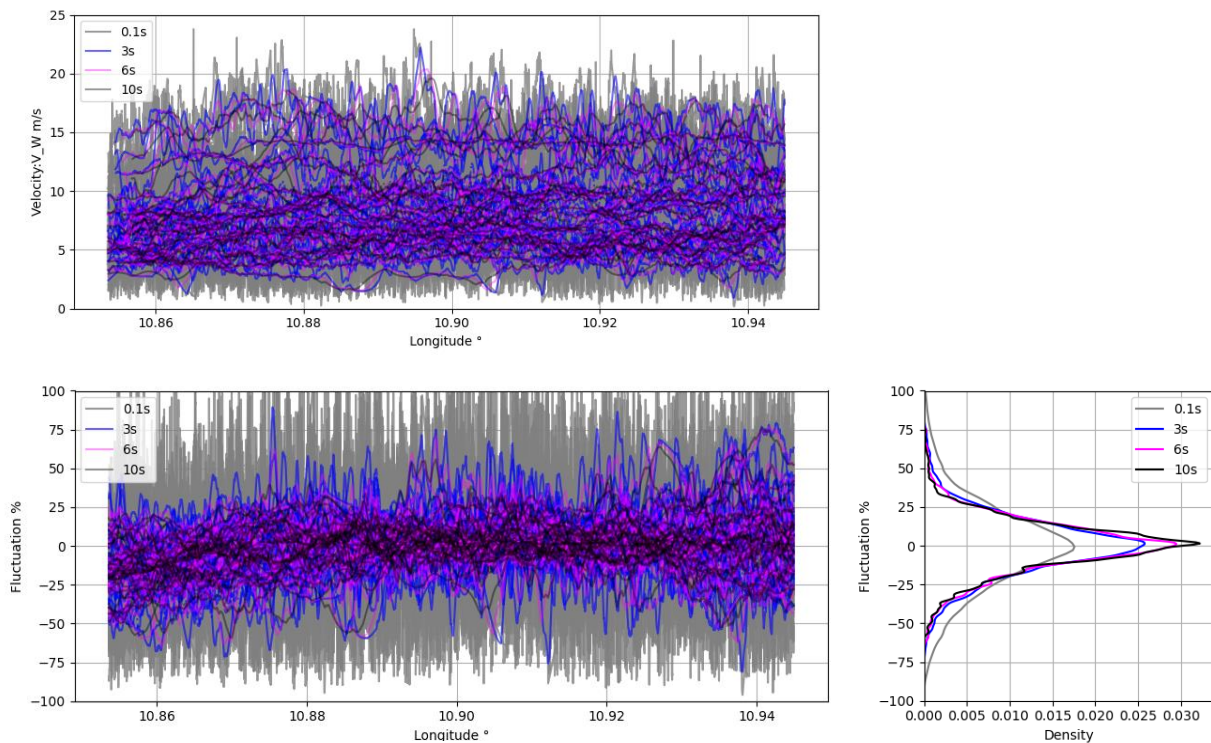


Figure 71: Velocity, normalized and probability density data collated from 30 measurements with crosswinds > 5m/s

The probability density of the collated 30 crosswind runs is presented in Figure 71 (right), with a zoomed in plot of the upper range in Figure 72. Although there is relatively low probability density at the upper range of fluctuations, there is the possibility of gusts with 3s, 6s and even 10s duration (corresponding to the respective moving averages) with fluctuation magnitudes of 50-80% above the mean over the entire bridge.

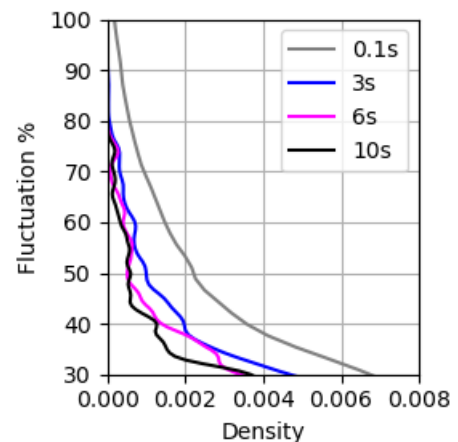


Figure 72: Upper range of probability density

### Velocity Range Sensitivity

The general characteristics identified have been observed only with the conditions during the bridge-crossing measurements were obtained. The sensitivity of these general characteristics to mean wind speed is investigated in this section. The range of which bridge-crossing measurements were obtained and processed are visible in Figure 71 (upper), ranging from crosswinds of ~5m/s to ~16m/s. To assess the sensitivity of the characteristics to wind speed, the 30 runs were divided into medium (5-10 m/s) and high (>10m/s) groups, each with at least 10 individual measurements, and then collated. The grouped medium and high crosswind measurements are presented in Figure 73 (upper), with the corresponding normalized values and probability density in Figure 73 (lower), Figure 73(right) respectively.

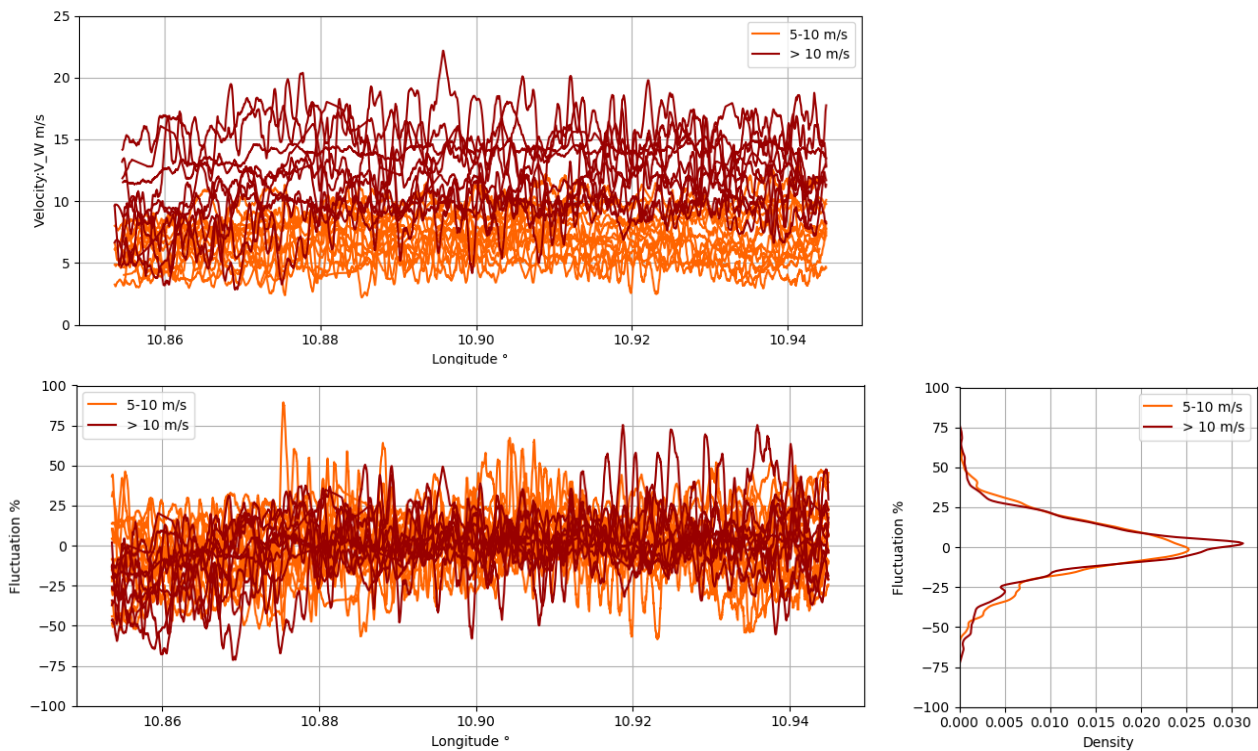


Figure 73: Velocity, normalized and probability density data collated from the two different velocity groups

The normalized velocity in Figure 73 (lower), probability density in Figure 73 (right), and particularly the upper range of the probability density in Figure 74 demonstrate that there is limited sensitivity of the general crosswind characteristics to the mean wind speed. The time-varying velocity exhibit similar fluctuation magnitudes, and gust profiles, as well as similar probability density of possible fluctuation magnitudes.

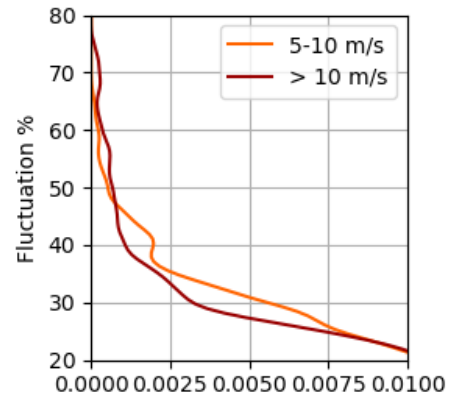


Figure 74: Upper range of probability density of the two different velocity groups

## Overview

In this section, specific quantities of interest of the general crosswind characteristics will be quantified. The concept of percentile is a relatively easy to interpret statistic that can describe the occurrence of the different gust magnitudes (in % fluctuation). The 95<sup>th</sup> percentiles are:

- 3 sec 95th percentile: +31.89% fluctuation
- 6 sec 95th percentile: +28.05% fluctuation
- 10 sec 95th percentile: +26.15% fluctuation

The 3 sec 95th percentile value for example, can be interpreted as: 5% of measurements (where mean crosswind >5m/s) had gusts of 3 second duration with fluctuation of at least +31.89% than the mean (~5min duration) across the whole bridge.

The percentiles for 3s, 6s and 10s are illustrated in Figure 75 (left), with 95% highlighted, with the corresponding fluctuations also highlighted in the probability density in Figure 75 (right).

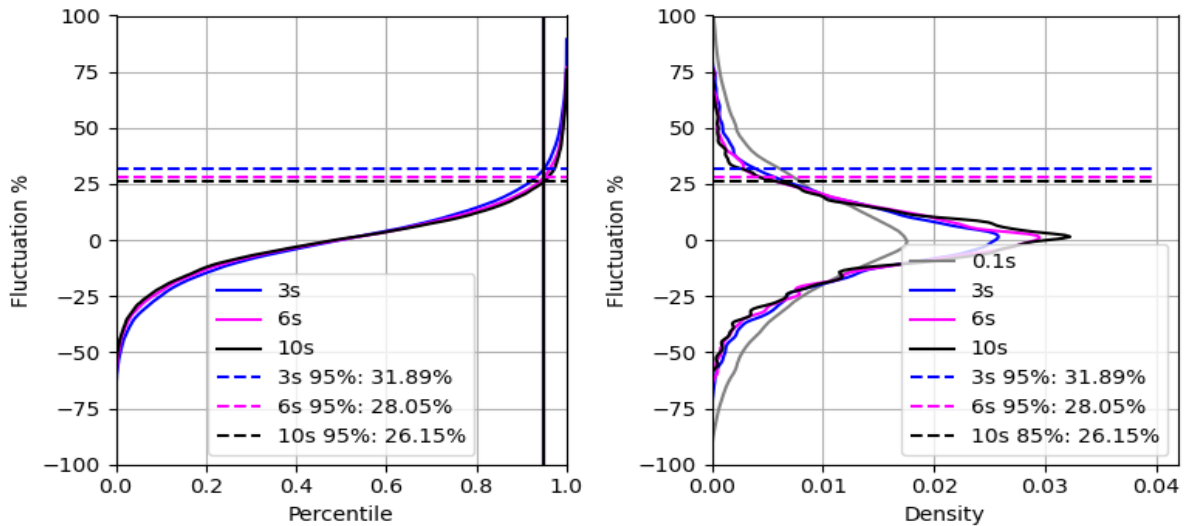


Figure 75: Percentile profiles with 95<sup>th</sup> percentile highlighted with corresponding probability density profiles

A 3 sec gust with a fluctuation magnitude of 25% corresponds to:

- 3 sec +25% fluctuation: 91.25th percentile

This statistic be interpreted as:

Fluctuations of +25% higher than the mean (~5min duration) across the whole bridge with a duration of 3 sec or longer, corresponds to the top 8.75 percentile of measurements (where mean crosswind >5m/s) – this is also illustrated in Figure 76.

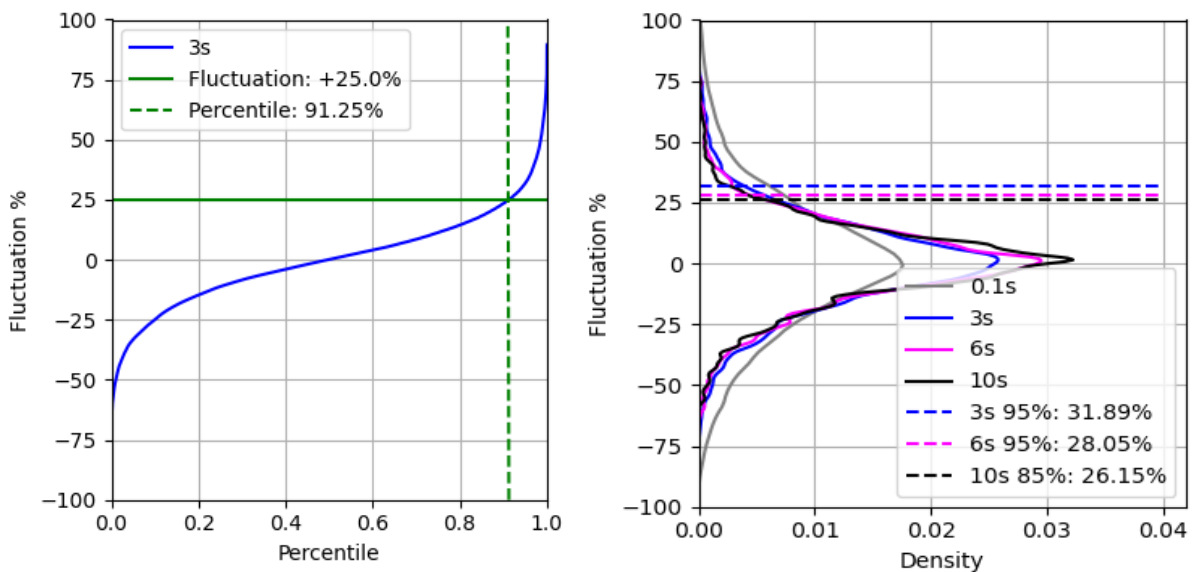


Figure 76: Percentile profiles with +25% fluctuation highlighted with corresponding probability density

## Conclusions

A detailed experimental campaign taking aerodynamic measurements over the Great Belt Bridge has been completed. These measurements were performed using the DLR FR8-LAB measurement container, a 'swap-body' fitted with a self-contained data acquisition, power supply and a communication system, transported on normal operating freight-trains. Measurements were performed over bridge from Jan 10<sup>th</sup> – March 4<sup>th</sup>, 2022.

Surface pressure measured on the FR8-LAB during operation were processed to derive the atmospheric wind a train/container is exposed to crossing the bridge. This was achieved utilizing a methodology developed for this investigation with a calibration in a 1:15 scale wind-tunnel experiment completed in April 2022.

The FR8-LAB measurements and methodology used to derive the wind velocity were validated against ultrasonic anemometer measurements also on-board operational freight trains performed by DB Systemtechnik, showing strong agreement.

Analysis of the bridge-crossing measurements identified that individual runs demonstrate time-varying characteristics:

- Significant velocity fluctuations around the ~5min mean during bridge crossings
- Significant variation between different, individual bridge-crossing measurements

In addition, general crosswind characteristics, developed from the collation of 30 bridge measurements (wind>5m/s) exhibited:

- Normalized fluctuations (% relative to mean across bridge) of 25-50 %
- 5% of measurements (where mean crosswind >5 m/s) had gusts of 3 second duration with fluctuation of at least +31.89 % than the mean (~5 min duration) across the whole bridge.
- Fluctuations of +25 % with a duration of 3 sec or longer, correspond to the top 8.75 percentile of measurements (where mean crosswind >5 m/s)

If the data would be extrapolated, this would result in:

- At a 5 min. mean velocity of 20 m/s, a 3 second averaged wind speed would be higher than 26.38 m/s with a probability of 5% during the bridge crossing.
- At a 5 min. mean velocity of 15 m/s, a 3 second averaged wind speed would be higher than 19.8 m/s with a probability of 5% during the bridge crossing.

## Appendix

The derived velocity profiles from the 30 measurements made with mean crosswinds >5m/s are presented here. In some cases, there are sections where data acquisition has temporarily failed, and the entire bridge crossing was not captured. These were included in the analysis as they represent useful data, particularly for transient analysis of peak velocities, as well as the general crosswind distribution analysis.

